

https://dspace.org/

Modelling the effect of carbon nanotube concentration on hydrophilicity of functionlized carbon nanotube infused polysulfone membrane

Aberefa, Oluseyi Adebisi

2015-06-01
http://hdl.handle.net/10539/18384

Downloaded from a DSpace repository. https://dspace.org/

MODELLING THE EFFECT OF CARBON NANOTUBE CONCENTRATION ON HYDROPHILICITY OF FUNCTIONALIZED CARBON NANOTUBE INFUSED POLYSULFONE MEMBRANE

Oluseyi Adebisi Aberefa

A research report submitted to the Faculty of Engineering and the Built Environment, University of Witwatersrand, Johannesburg, in partial fulfilment of the requirements for the degree of Master of Science in Engineering

Johannesburg, 1 June 2015

DECLARATION

I declare that this research report is my own, unaided work. It is being submitted for the degree of Master of Science in Engineering at the University of the Witwatersrand, Johannesburg. It has not been submitted before for any degree or examination in any other University.

Oluseyi Adebisi Aberefa

…… Day of …….. 2015

ABSTRACT

The need for a mathematical relationship between carbon nanotube (CNT) concentration and hydrophilicity of nanocomposites (during the purification process of water-oil mixture) is essential for research in the area of membrane separation. In this study, the effect of CNT concentration on hydrophilicity of functionalized CNT-infused polymeric membrane was reviewed and a mathematical model that can effectively predict the contact angle of functionalized CNT-infused polysulfone membrane for water-oil treatment was developed. Hydrophilicity tests were performed on the functionalized CNT-infused polysulfone membrane by sessile drop method using Goniometer at CNT concentration of 0%; 0.04%; 0.08%; 0.1%; 0.2%; 0.3% and 0.4 wt%. The results showed that the contact angle of the synthesized membrane decreased with increase in CNT content. This confirmed that the hydrophilicity of the membrane was enhanced by the addition of functionalized CNTs. A symbolic regression model was then used to predict correlations between the CNT concentration and the contact angle of the nanocomposite membrane using Eureqa^{TM} (desktop version 0.99.9) software.

The Nutonian models using Eureqa^{TM} software were then subjected to verification to select the best model based on complexity-to-accuracy Pareto, error metrics and sensitivity tests. The selected model was adjusted based on the underlying model assumptions. The final model was tested for adequacy by means of standard deviation, σ and percentage absolute average relative error, %AARE using a new set of experimental data outside the region of data space used for the model development. The results showed that standard deviation, σ and %AARE of the model output against the validating experimental data are 0.017 and 2.09%, respectively. This indicates that the model is adequate to predict hydrophilicity of functionalized CNT-infused polysulfone membrane (irrespective of the method of functionalizing CNT and the polysulfone membrane base solvent used).

DEDICATION

Dedicated to God Almighty, the one in whom we have our being and our sufficiency.

ACKNOWLEDGEMENTS

I would like to take this opportunity to express my sincere gratitude to those who helped throughout this project.

My special thanks go to my supervisor, Dr. B. D. Nkazi for his commitment, guidance, advice and numerous hours spent helping me on this work…thank you Dr. Nkazi! To my co-supervisor, Prof S. E Iyuke, you are a mentor and a father…thank you for believing in me and for your great assistance, I am short of words.

I like to thank my colleagues in the Petroleum Engineering Unit: Aliki, Lerato, Tsepo, Sbusiso, Derrick, Kwame, Thendai, Kingley and Palesa. Each of you contributed significantly to my life during the course work part of this programme, especially my dear friend Palesa, I am grateful for all your help, thank you.

To the members of staff of Aleph Learning Academy Secunda, I am thankful. Especially to the CEO, Dr. Moore, your support is enormous, thank you for all your help.

The financial contribution by CHIETA to the research study is gratefully acknowledged. Many thanks to Nutonian Inc. USA for providing a free license to use their software, Eureqa™.

Finally, I like to thank my dearest wife, Funke and my children: Praise, Wisdom and Michelle. You created an enabling environment for me to study; the measure of your support can not be quantified. Thank you for loving me the way I am.

TABLE OF CONTENTS

DECLARATION……i

ABSTRACT……..ii

DEDICATION...……iii

ACKNOWLEDGEMENTS....……...iv

TABLE OF CONTENTS …….……v

LIST OF FIGURES....……..……....vii

LISTOF TABLES....……viii

NOMENCLATURE……..ix

CHAPTER ONE – INTRODUCTION……..1

1.1 Introduction ...……1

1.2 Problem statement ……3

1.3 Research objective ...……..3

1.4 Research approach ...……..4

1.5 Report outline ...……....5

CHAPTER TWO – LITERATURE REVIEW……7

2.1 Carbon nanotubes (CNTs) and their properties..……...7

2.2 Functionalization of CNTs....……9

2.2.1 Chemical functionalization....……9

2.2.1 Physical functionalization....……10

2.3 Influence of functionalized CNTs on polymeric membrane....……12

2.3.1 Dispersion...……...12

2.3.2 Hydrophilicity……13

2.4 Effect of CNT concentration on hydrophilicity of functionalized CNT infused polymeric membrane....……14

2.5 Methods of measuring contact angle.....……..17

2.5.1 Wilhelmy plate method....……..17

2.5.2 Goniometry…….....18

2.6 Mathematical models for contact angle prediction……..……..19

2.6.1 Laplace-Young model……...19
2.6.2 Hough transformation algorithm……...21
2.6.3 Shikhmurzaev's model……..21

CHAPTER THREE – MODELLING PROCEDURE……23

3.1 Introduction……23
3.2 Problem definition……...23
3.2.1 Model objective……23
3.2.2 System analysis……25
3.3 Data collection…….....25
3.4 Data analysis……25
3.5 Model verification and validation…….....26

CHAPTER FOUR- RESULTS AND DISCUSSION……..29
4.1 Results……..29
4.2 Discussion……32

CHAPTER FIVE – CONCLUSION AND RECOMMENDATIONS…...……35
5.1 Conclusion……35
5.2 Recommendations……36

REFERENCES……..37

APPENDIX A: Experimental data analysis……45
APPENDIX B: Model development……...47
APPENDIX C: Models error metrics…..……54
APPENDIX D: Models sensitivity reports…..……61
APPENDIX E: Models statistical reports..……65

LIST OF FIGURES

Figure 1.1 Relationship between membrane permeability and selectivity for polymeric membrane…… 1

Figure 1.2 Schematic of research approach to developing and validating the model……. 5

Figure 2.1 Graphene sheet rolled to make capped single wall carbon nanotube..…….. 7

Figure 2.2 Formation of different types of CNTs (A: armchair; B: zigzag; C: chiral)….. 8

Figure 2.3 Schematics of different physical methods of CNT functionalization (A: polymer wrapping; B: surfactant adsorption; C: endohedral method)……. 11

Figure 2.4 Surface contact angle of the hydroxyl functionalized CNTs/polyacylonitrile membrane……..... 17

Figure 2.5 Schematic diagram of the Wilhelmy plate method from Kruss GmbH..…… 18

Figure 2.6 Coordinate system for an axisymmetric drop……..……... 19

Figure 3.1 Schematic diagram of route through the stages of modelling……. 24

Figure 4.1 complexity-to-accuracy Pareto of the selected model…….. 30

Figure 4.2 Model fit against the experimental data…….. 31

Figure 4.3 Model fit against the validating experimental data……. 31

Figure B1 Screen shot of enter data tab of Eureqa……... 47

Figure B2 Screen shot of prepare data tab after smoothing x variables……... 48

Figure B3 Screen shot of prepare data tab after smoothing y variables……... 49

Figure B4 Screen shot of define search tab…….. 51

Figure B5 Screen shot of start search tab……. 52

Figure B6 Screen shot of the Result tab……... 53

LIST OF TABLES

Table 2.1 Thermal and Electrical properties of different carbon materials…….. 9

Table 2.2 Summary of various CNT functionalization methods……. 12

Table 2.3 Static contact angles and porosity of the amine-functionalized multi-walled CNTs/ polyethersulfone membrane…….. 14

Table 2.4 Contact angle and Pore size of the ICIC functionalized CNTs/Polysulfone membrane……. 15

Table 2.5 Contact angle and Pore size of the amide functionalized CNTs/Polysulfone membrane……. 16

Table 3.1 Experimental data used for the model development…… 26

Table 4.1 Error metrics for the model equation……29

Table 4.2 Model output versus experimental data……... 30

Table 4.3 Standard deviation and AARE calculation parameters for model validation...32

Table A1 MAD of the experimental contact angle at CNT concentration of 0 wt%..... 45

Table A2 MAD of the experimental contact angle at CNT concentration of 0.04 wt%... 45

Table A3 MAD of the experimental contact angle at CNT concentration of 0.08 wt%... 45

Table A4 MAD of the experimental contact angle at CNT concentration of 0.10 wt%... 46

Table A5 MAD of the experimental contact angle at CNT concentration of 0.20 wt%... 46

Table A6 MAD of the experimental contact angle at CNT concentration of 0.30 wt%... 46

Table A7 MAD of the experimental contact angle at CNT concentration of 0.40 wt%... 46

NOMENCLATURE

AARE	Absolute average relative error
ARE	Average relative error
$CdCl_2$	Cadmium chloride
CdI_2	Cadmium iodide
C_h	Chiral vector
CNT/CNTs	Carbon nanotube/carbon nanotubes
DMF	Dimethylformamide
DWCNT	Double-walled carbon nanotube
MAD	Mean absolute deviation
MMM	Mixed matrix membrane
MWCNT	Multi-walled carbon nanotube
nm	Nanometer
PbI_2	Lead iodide
PSF	Polysulfone
RE	Relative error
SWCNT	Single-walled carbon nanotube
$ThCl_4$	Thorium Tetrachloride
$TiCl_4$	Titanium tetrachloride
V and V	Verification and validation
wt	Weight
µm	Micrometer

CHAPTER ONE

INTRODUCTION

1.1 Introduction

Polymeric membranes have shown advantages for necessary mechanical properties and efficient handling capabilities (Shimekit et al., 2010). However, existing polymeric membrane materials seem to have reached a maximum level of compromise between permeability and selectivity and thus are inadequate to wholly exploit commercialization opportunities. The problem is if one increases permeability, selectivity decreases and vice versa (WIPO, 2009), as shown in Figure 1.1.

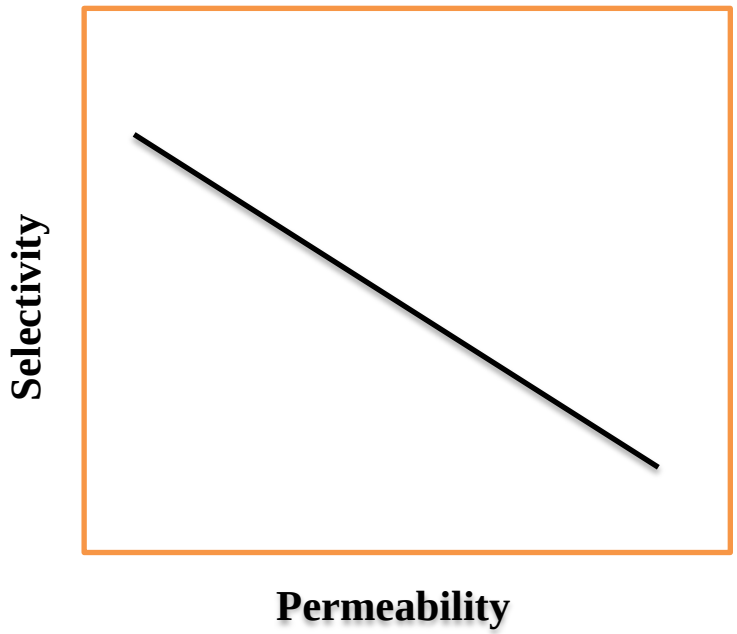


Figure 1.1: Relationship between membrane permeability and selectivity for polymeric membrane

A considerable amount of research effort has placed emphasis on adding inorganic materials such as zeolites and carbon molecular sieves to polymers in order to improve the efficiency of polymeric membranes (Shimekit et al., 2010). These are known as mixed matrix membrane (MMM). MMM takes advantage of desirable properties of inorganic molecular sieves alongside the necessary mechanical and handling capabilities of polymers. However, the successful integration of zeolites in

MMM is affected by poor interfacial adhesion of the zeolite with the polymer, causing un-selective voids in the membrane (Kim et al., 2007).

After the report on carbon nanotubes (CNTs) by a renowned Japanese scientist, Iijima (1991), CNTs have been studied broadly by researches in different disciplines. CNTs are one dimensional carbon materials whose aspect ratio is greater than 1000 (Kim et al., 2007) and have mechanical properties that surpass those of any existing materials (Yakobson and Avouris, 2001). CNTs/polymer composites have been praised for having extraordinary features like strength, stiffness, chemical inertness, damping properties, electrical/thermal properties, light weight etc. in comparison to standard composites (Inam and Peijs, 2007).

In membrane filtration, two major problems are encountered which are fouling and concentration polarization (Wu et al., 2010). While fouling is the build-up of substances on the surface and/or inside the membrane pores, concentration polarization is the accumulation and creation of a layer of substances near the membrane surface due to slow or non-permeation of the components. These factors reduce the performance of the membrane (Maphutha et al., 2013).

Several methods have been proposed in literatures to control the membrane fouling, these include but are not limited to: choice of a proper membrane material, pre-treatment of the process fluid, modification of operating parameters and using back washing and back pulsing (Vatanpour et al., 2014). However, the major factor in the fouling of the membranes is their surface characteristics (Rana and Matsuura, 2010). It is generally accepted that the more hydrophilic a membrane is the better its fouling resistance based on the fact that most fouling agents are naturally hydrophobic (Park et al., 2014). One of the ways of modifying the membrane surface characteristic is by using functionalized CNTs to increase its hydrophilicity.

While CNTs have exceptional mechanical properties, the practical incorporation of CNTs into polymeric membranes has suffered major problems which include but are not limited to: dispersion, alignment, agglomeration, re-agglomeration, interfacial adhesion and control of CNT structure (Inam and Peijs, 2007). The dispersion challenges encountered in CNTs is quite different from that of conventional fillers, like spherical particles and carbon fibers because CNTs have a very large surface area

due to the high aspect ratio and small diameter (in nanometer scale) (Ma et al., 2010). The outer wall of pure CNTs is presumed to be chemically inert technically and is not capable of providing an effective stress transfer across the CNT-matrix interface. One of the best ways of overcoming these difficulties is to functionalize CNTs (Chen et al., 2008).

A number of methods have been discussed in the literature to measure the hydrophilicity of a nanocomposite membrane via contact angle measurement. These methods include sessile drop method by a contact angle Goniometer, Washburn capillary rise method, Wilhelmy plate method and vibration-induced method (Pegoretti et al., 2008). A contact angle is the leading angle formed by a liquid droplet being used and the tangent to the droplet interface at the obvious intersection between a liquid-vapour interface and a solid surface. This intersection is called the contact line (Russell, 2009). The accuracy of methods of contact angle measurement is largely dependent on smoothness of the membrane surface hence, a need for a mathematical model to accurately predict contact angle without a dependence on imaging of the contact line.

1.2 Problem Statement

In order to predict the hydrophilicity of nanocomposite membrane, the development of a mathematical model is required. This problem can be solved through investigating the relationship between the CNT concentration and hydrophilicity of nanocomposites during the purification process of a water-oil mixture. Therefore, answers should be made to the following fundamental questions. Firstly, “How do one explain CNT content - hydrophilicity interactions in membrane separation process in terms of rejection?” Secondly, “How do one incorporate the knowledge into the development of a mathematical relationship?” This is the fundamental system analysis upon which this research is based.

1.3 Research Objectives

The specific research objectives are:

- Review the effect of CNT concentration on hydrophilicity of functionalized CNT- infused polymeric membranes.

- Develop a mathematical model that can effectively predict the contact angle (hydrophilicity test) of functionalized CNT-infused polysulfone membranes for water-oil treatment.
- Verify and validate the model using statistical model validation techniques.

1.4 Research Approach

Previously synthesized functionalized CNT-infused polysulfone membranes within the Nanotechnology Research Group (at different CNT concentrations) were used to determine the experimental relationship between CNT concentration and hydrophilicity. The data would then be analysed using two approaches:

- Data Cleaning- This approach includes identifying and correcting errors in the data. It also involves filling in the missing variables in the data using the linear regression computational method.

- Data Sub-grouping- This approach involves selection of a subgroup of variables relevant for the modelling from the original variables using the least absolute deviation from the mean statistical method.

Then, Eureqa™ software was used to predict the relationship between CNT concentration and hydrophilicity. The models from Eureqa™ were then subjected to verification and validation (V and V), using statistical model V and V techniques until an accurate model was achieved. The schematic diagram of the approach is shown in Figure 1.2.

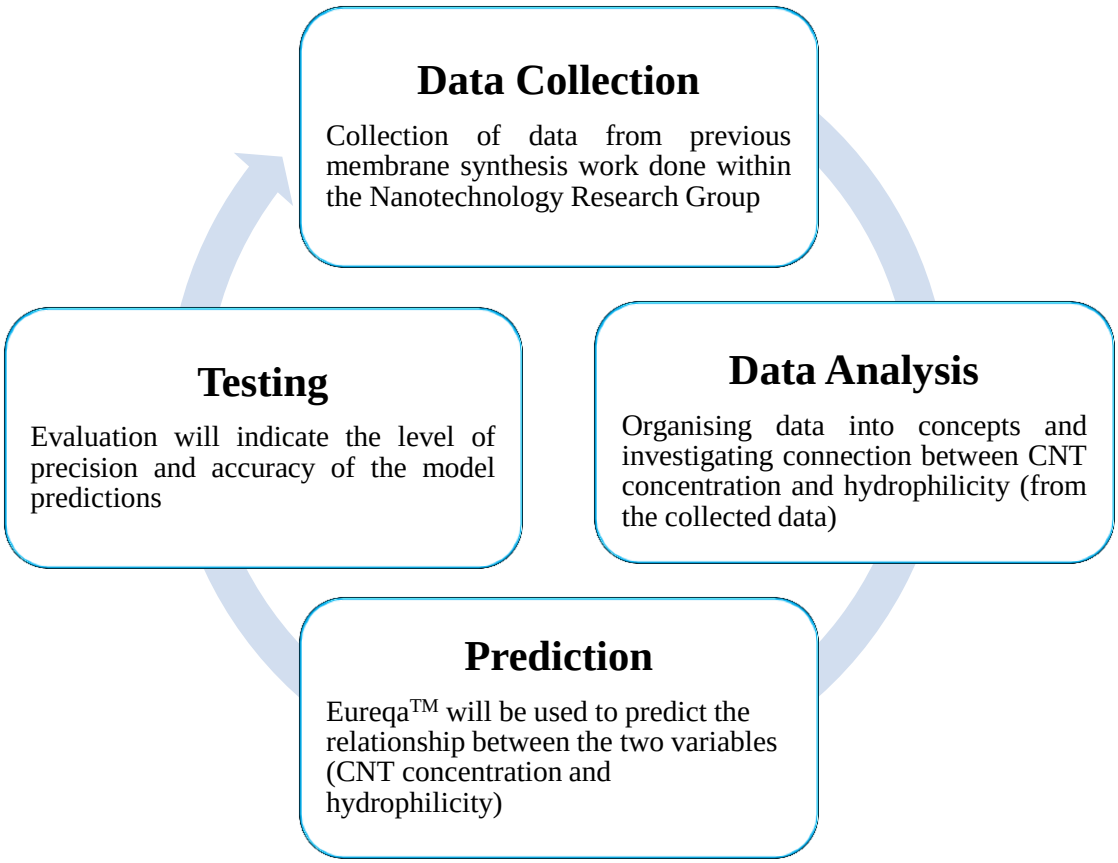


Figure 1.2: Schematic of research approach to developing and validating the model

1.5 Report Outline

This research report is divided into 5 chapters:

Chapter 1: The motivation for the research, research objectives and the approach adopted for the research are in this chapter.

Chapter 2: This chapter gives an overview of CNTs, functionalization of CNTs and the effect of functionalized CNT concentration on nanocomposite membranes. The chapter also includes a review of methods and mathematical models for contact angle measurement.

Chapter 3: This chapter describes the process used for the model development.

Chapter 4: This chapter contains the results of the model and discussion of the outcomes.

Chapter 5: The conclusion of the research report with a summary of the findings (and recommendations) are presented in this chapter.

CHAPTER TWO

LITERATURE REVIEW

2.1 Carbon nanotubes (CNTs) and their properties

To bring the structure of a CNT into perspective, one could imagine it as a rolled up sheet of graphene with planar-hexagonal distribution of carbon atoms arranged in a honeycomb lattice as shown in Figure 2.1 (Chen et al., 2011). CNTs are grouped into single-walled carbon nanotube (SWCNT), double-walled carbon nanotube (DWCNT), and multi-walled carbon nanotube (MWCNT) based on the number of rolling layers of graphene sheets (Peponi et al., 2011).

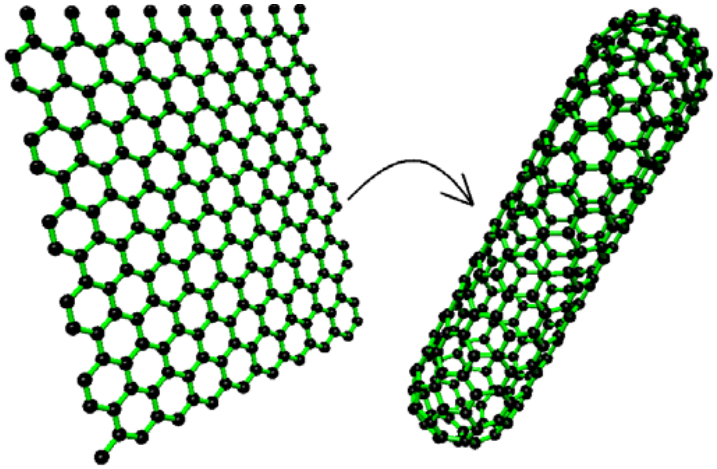


Figure 2.1: Graphene sheet rolled to make capped single wall carbon nanotube (Chen et al., 2011)

Ma et al. (2010) describe three types of CNTs viz armchair, zigzag and chiral (based on the rolling angle of the graphene sheet). Figure 2.2 shows various types of CNTs formed from planar-hexagonal graphene sheet as given by chiral vector Equation (2.1):

$$C_h = na_1 + ma_2 \quad (2.1)$$

Where the integers (n, m) are the number of movements along the unit vectors (a_1 and a_2) of the hexagonal lattice.

Using this (n, m) naming system, three kinds of orientation of the carbon atoms around the nanotube circumference arise. If n = m, the nanotubes are called ‘‘armchair”. If m = 0, the nanotubes are ‘‘zigzag”. Otherwise, they are termed ‘‘chiral”.

According to Kirtania and Chakraborty (2012), the circumference of CNTs can be determined using Equation (2.2):

$$L = a\sqrt{n^2 + m^2 + nm} \qquad (2.2)$$

Where ‘a’ is the length of the unit vector.

The chiral angle (θ) of the chiral vector is determined using Equation (2.3):

$$\cos\theta = \frac{(n+m)/2}{\sqrt{n^2+m^2+nm}} \qquad (2.3)$$

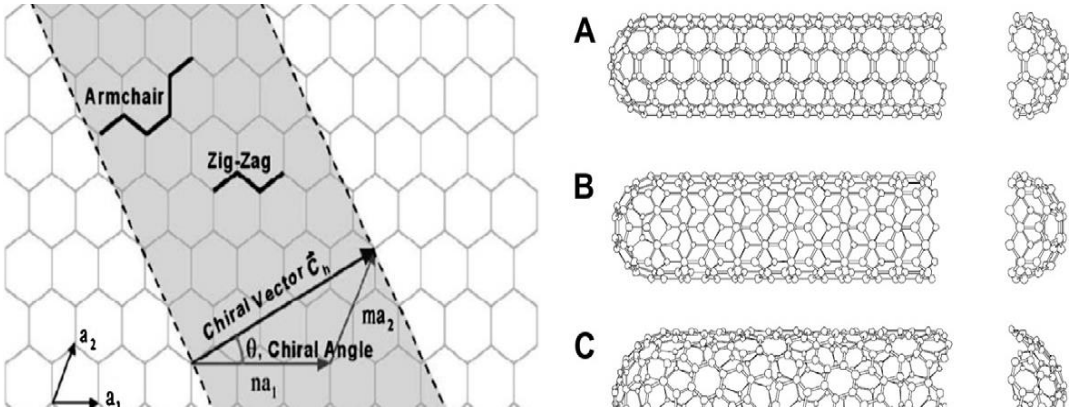


Figure 2.2: Formation of different types of CNTs (A: armchair; B: zigzag; C: chiral) (Ma et al., 2010)

After Iijima’s report on CNTs in 1991 (Iijima, 1991), researchers in various fields have been attracted by the outstanding combination of electrical, thermal and mechanical properties of CNTs. The elastic modulus and tensile strength were theoretically predicted to be as high as ~2 TPa and ~200 GPa, respectively (Du et al., 2007). Table 2.1 shows the superior thermal and electrical properties of CNTs over other carbon materials.

Table 2.1: Thermal and electrical properties of different carbon materials (Ma et al., 2010)

Properties	**C materials**				
	Graphite	Diamond	Fullerene	SWCNT	MWCNT
Specific gravity (g/cm3)	1.9–2.3	3.5	1.7	0.8	1.8
Electrical conductivity (S/cm)	4000^{p}, 3.3^{c}	$10^{-2} – 10^{-15}$	10^{-5}	10^{2} -10^{6}	10^{3} -10^{5}
Electron mobility (cm2/ (V s))	2.0 x 10^{4}	1800	0.5 – 6	~10^{5}	10^{4}-10^{5}
Thermal conductivity (W/(m K))	298^{p}, 2.2^{c}	900-2320	0.4	6000	2000
Coefficient of thermal expansion (K^{-1})	-1 x 10^{-6p} 2.9 x 10^{-5c}	(1~3) x 10^{-6}	6.2 X 10^{-5}	Negligible	Negligible
Thermal stability in air (^{o}C)	450–650	< 600	~ 600	> 600	> 600

2.2 Functionalization of CNTs

The agglomerating nature of CNTs, due to van der Waals force makes it difficult for them to dissolve in solvents (whether aqueous or non-aqueous) even in the presence of dispersing materials (Inam and Peijs, 2007). This imposes a huge restriction to the commercial use of CNTs. Therefore, surface functionalization of CNTs is a major area of research (Chen et al., 2011). Several methods that explain the chemistry of functionalized CNTs and the reaction mechanisms linking the CNTs and functional groups have been proposed in the literature. These methods are grouped into two namely, chemical and physical methods of functionalization, depending on the interfaces between the active molecules and carbon-carbon atoms of the CNTs (Ma et al., 2010; Rafiee and Pourazizi, 2014).

2.2.1 Chemical (covalent) functionalization

Chemical functionalization covalently connects functional entities onto the carbon scaffold of CNTs. This could be done by direct covalent sidewall functionalization or by defect transformation.

(i) Direct sidewall method: This is based on modification of the hybridization of carbon atom from sp^2 to sp^3 and an instantaneous loss of π-conjugation arrangement on the graphene layer. However, this method has been discovered to damage the

essential properties of SWCNTs and has the potential for secondary agglomeration of CNTs in polymer matrix (Inam and Peijs, 2007; Chen et al., 2011).

(ii) Defect functionalization method: This method uses the principle of a chemical change of defect sites on CNTs. Defect sites can be the open ends and/or holes in the sidewalls of hexagon graphene framework or by pre-oxidization of CNTs (Ma et al., 2010). CNTs can be pre-oxidized to create a defected site by using strong acids such as nitric acid, sulfuric acid, or a mixture of them; or with strong oxidants such as potassium per manganite in acidic medium, ozone or reactive plasma (Dyachkova et al., 2013).

The defects on CNTs formed by oxidants are subjected to secondary functionalization by attachment with carboxylic acid (–COOH), amine ($-NH_2$), or hydroxyl (–OH) groups (De Lannoy et al., 2013). Additionally, long alkyl chains have been covalently bonded onto oxidized CNTs by an amidation reaction (Lin et al., 2003). Furthermore, chemical reactions of the defected CNTs with molecular fluorine, rhodamine B, and p-carboxytetraphenylporphine have been studied (Tasis et al., 2006). These functional groups have interesting chemistry and the CNTs can be used as building block for subsequent chemical reactions (Ma et al., 2010).

2.2.2 Physical (non-covalent) functionalization

Physical functionalization of CNTs has to do with self-assembly of individual CNTs to thermodynamically stable structures that are held together by non-covalent bonds (Lin et al., 2003). Some of the methods that have been extensively used include: non-covalent polymer wrapping by various species of polymers, surfactant adsorption and endohedral filling.

(i) Polymer wrapping: High molecular weight polymers such as hydrocarbon and conjugated polymers the have potential to wrap around the surface of CNTs to form super molecular complexes of CNTs (Yang et al., 2011). This is due to the suspension of CNTs in the presence of polymers, for example, polypropylene, polyethylene and polystyrene (Tasis et al., 2006). This is a very good example of physical functionalization of CNTs with no damage to the structure and original properties of the CNTs (Figure 2.3A and Table 2.2). The van der Waals interactions and p–p

stacking between CNTs and polymer chains having aromatic rings enables the polymer wrapping process (Ismail et al., 2009).

(ii) Surfactant adsorption: Surfactants have been used for CNTs functionalization (Rahimpour et al., 2012). The physical adsorption of surfactant on the CNT surface reduced the surface tension of CNT thereby, successfully preventing the formation of aggregates (Figure 2.3B). In addition, the surfactant-treated CNTs overcome the van der Waals attraction by electrostatic repulsive forces (Wang et al., 2014). The effective adsorption of surfactants on CNTs depends strongly on the properties of surfactants, medium chemistry and polymer matrix (Bekou and Mattia, 2011).

(iii) Endohedral filling: This method uses the principle of the capillary effect. The foreign atoms are inserted into the inner cavities of CNTs through the capillary effect (Tasis et al., 2006). The insertion mostly takes place at defect sites contained at the ends or on the sidewalls (Figure 2.3C). The filling of the inner cavities of CNTs worked with fullerene derivatives and inorganics as encapsulated species. Additionally, insertion of metal halides into the tubes, such as $AgCl_xBr_y$, CdI_2 and $ThCl_4$, $CdCl_2$, $TbCl_3$, $TiCl_4$ and PbI_2, is a good example of functionalization by Endohedral method (Hirsch, 2002).

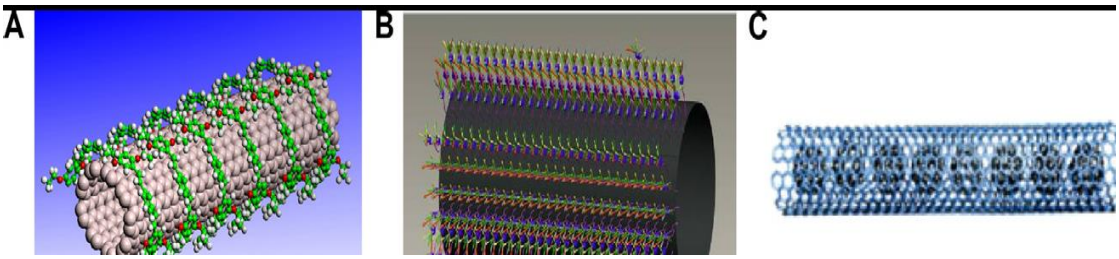


Figure 2.3: Schematics of different physical methods of CNT functionalization (A: polymer wrapping; B: surfactant adsorption; C: endohedral method), (Hirsch 2002)

Table 2.2: Summary of various CNT functionalization methods

Method		Principle	Possible damage to CNTs	Easy to use	Interaction with polymer matrix[a]	Re-agglomeration of CNTs in matrix
Chemical method	Side wall	Hybridization of C atoms from sp^2 to sp^3	Yes	No	S	Yes
	Defect	Defect transformation	Yes	Yes	S	Yes
Physical method	Polymer wrapping	Van der Waals force, л-л stacking	No	Yes	V	No
	Surfactant adsorption	Physical adsorption	No	Yes	W	No
	Endohedral method	Capillary effect	No	No	W	Yes

[a] S: Strong; W: Weak; V: Variable; depending on the miscibility between matrix and polymer on CNT **(**Ma et al., 2010).

2.3 Influence of functionalized CNTs on polymeric membrane

Two key influences of functionalized CNTs on polymeric membrane are: improved dispersion of CNTs in polymers thereby, enhancing effective stress transfer across CNT/polymer matrix and improved hydrophilicity of CNT/polymer composite for better oil/water ultrafiltration.

2.3.1 Dispersion

One of the fundamental challenges of CNT/polymer composite preparation is uniform dispersion of CNTs in the polymers (Naderi, 2013). Several factors are responsible for difficult dispersion of CNTs in a polymer matrix. These include the fact that CNTs are produced in bundles and the attraction between CNTs by van der Waals forces cause the CNTs themselves to tend to agglomerate (Zhao et al., 2012).

The strong van der Waal force between CNT-CNT surfaces weakens the interfacial bonding between CNTs and the polymer matrix. This will reduce effective stress transfer across the CNT/polymer structural composite (Jogi et al., 2012). The CNT/polymer composites obtained have poor mechanical properties and their intrinsic properties cannot be realized (Du et al., 2007).

The dispersion challenges encountered in CNTs is quite different from that of conventional fillers, like spherical particles and carbon fibers because CNTs have

very large surface area due to the high aspect ratio and small diameter in nanometer scale (Ma et al., 2010; Kumar and Ulbricht, 2014). The outer wall of pure CNTs is presumed to be chemically inert technically, and is not capable of providing an effective stress transfer across the CNT-matrix interface. One of the best ways of overcoming these difficulties is to functionalize CNT (Chen et al., 2008).

While CNT functionalization enhanced the dispersion and interfacial adhesion between CNTs and polymer matrix it also has some negative effects on the CNT (Majeed et al., 2012). These include: disorientation of the bonding between graphene sheets, thereby reducing the intrinsic transport properties of CNTs in the final composite; and decrease in the contact between CNTs which reduces the final conductive properties of CNT/polymer composite. Especially for electronic application where the effective conducting CNT path and good contact between individual CNTs are of utmost importance (Du et al., 2007).

It is therefore advisable that since functionalization of CNTs is very important to the dispersion and interfacial interaction between CNT/polymer matrix (which is difficult to achieve through other means), it must be undertaken without damaging the intrinsic structure and adversely affecting the mechanical properties of CNTs.

2.3.2 Hydrophilicity

Two major problems which reduce the efficiency of membranes in membrane filtration are fouling and concentration polarization (Wu et al., 2010). Fouling is the build-up of substances on the surface and/or inside the membrane pores and concentration polarization is the accumulation and creation of layer of substances near the membrane surface due to slow or non-permeation of the components (Qiu et al., 2009; Maphutha et al., 2013).

Vatanpour et al. (2014) proposed that membrane fouling can be controlled through: selection of a proper membrane material, pre-treatment of the process fluid, modification of operating parameters and using back washing and back pulsing. However, the major factor in the fouling of the membranes is their surface characteristics (Rana and Matsuura, 2010). It is generally accepted that the more hydrophilic a membrane is the better its fouling resistance based on the fact that most fouling agents are naturally hydrophobic (Park et al., 2014). One of the ways of

modifying the membrane surface characteristic is by using functionalized CNTs to increase its hydrophilicity.

Chemical functionalization of CNTs is helpful for the introduction of hydrophilic functional group, like amine (Rahimpour et al., 2012), into the surface of the CNTs which will not only improve dispersion of CNTs into polymer matrix but also the hydrophilicity of the nanocomposite.

2.4 Effect of CNT concentration on hydrophilicity of functionalized CNT infused polymeric membrane

A number of papers have been published on the effect of CNT concentration on hydrophilicity of different functionalized CNT infused polymeric membranes. In the work of Vatanpour et al. (2014), amine-functionalized multi-walled CNTs was embedded in polyethersulfone membrane at 0.015%, 0.03%, 0.045% and 0.06 wt% concentrations.

The result showed that the contact angle dropped considerably with blending of the functionalized CNTs into the polymer matrix. The plain polyethersulfone membrane showed the highest contact angle of 64.5^{o}. Increase in functionalized CNT concentration added caused a decrease in the contact angle hence, higher hydrophilicity as shown in Table 2.3.

Table 2.3: Static contact angles and porosity of the amine-functionalized multi-walled CNTs/ polyethersulfone membrane, (Vatanpour et al., 2014)

CNT concentration (wt%)	Contact angle	Porosity
0.0	64.5	73.2 ± 0.9
0.015	58.0	79.5 ± 0.8
0.03	56.9	77.7 ± 1.1
0.045	55.5	75.4 ± 0.7
0.06	53.6	73.9 ± 1.2

Qiu et al (2009) functionalized MWCNTs by 5-isocyanato-isophthaloyl chloride (ICIC) and blended it with polysulfone membrane at 0.12%, 0.15%, 0.32% and 0.5 wt% concentrations. The static water contact angle of the blend membrane surface

decreased from 82^{o} to 71.2^{o} when the CNT concentration increased from 0 to 0.32%. This indicated that the hydrophilicity of the blend membrane improved with the increase in concentrations of functionalized CNTs which would cause an increase in pure water flux.

However, when CNT concentration exceeded 0.32 wt%, especially at concentration of ~ 0.5 wt%, contact angle of the blend membrane increased which showed a decrease in hydrophilicity. This could be due to high steric hindrance and electrostatic interactions between modified CNTs and polysulfone, or agglomeration of modified CNTs in the polymer matrix (Shah and Murthy, 2013). The high concentration of CNTs in the nanocomposite could decrease the porosity as shown in Table 2.4.

Table 2.4: Contact angle and pore size of the ICIC functionalized CNTs/polysulfone membrane (Qiu et al 2009)

CNT concentration (wt%)	Contact angle (^{o})	Pore size (nm)
0.00	82.0	5.2
0.12	80.5	18.6
0.15	77.5	25.7
0.32	71.2	34.1
0.50	74.5	30.3

Shah and Murthy (2013) synthesized amide functionalized CNTs with polysulfone membrane by the phase inversion method using dimethylformamide (DMF) as solvent and water (with isopropanol) as coagulant. The concentrations of functionalized CNTs in the nanocomposite were 0.1%, 0.2%, 0.5%, 0.7% and 1.0 wt%.

The results showed that the contact angle of the synthesized membrane surface decreased from 77.7^{o} to 26.7^{o} when the CNT concentration increased from 0 to 1.0%. This indicated that the hydrophilicity of the synthesized membrane improved with the increase in concentrations of functionalized CNTs. In addition, the pore size decreases from 0.1079 to 0.025 when the CNT concentration increased from 0 to 0.5%. However, the report indicated that the minimum pore size was reached at 0.5% of the

CNTs as no further reduction in pore size was achieved as more CNTs were added as shown in Table 2.5.

Table 2.5: Contact angle and pore size of the amide functionalized CNTs/polysulfone membrane (Shah and Murthy, 2013)

CNT concentration (wt%)	Pore size (μ)	Contact angle (^{o})
0.0	0.1079	77.7
0.1	0.028	77.6
0.2	0.026	77.6
0.5	0.025	77.5
0.7	0.025	76.3
1.0	0.025	26.7

In the work of Majeed et al. (2012), hydroxyl functionalized multi-walled CNTs were mixed with polyacylonitrile to prepare ultrafiltration membranes at three different concentrations of CNTs: 05%, 1.0% and 2.0 wt%.

It was observed that the surface hydrophilicity of the membrane was enhanced by the addition of hydroxyl functionalized CNTs. The contact angle of the membrane decreases with increase in the concentration of CNT as shown in Figure 2.4. However, an increase in contact angle was observed with the CNT concentration exceeding 1.0% which indicated a decrease in the membrane hydrophilicity.

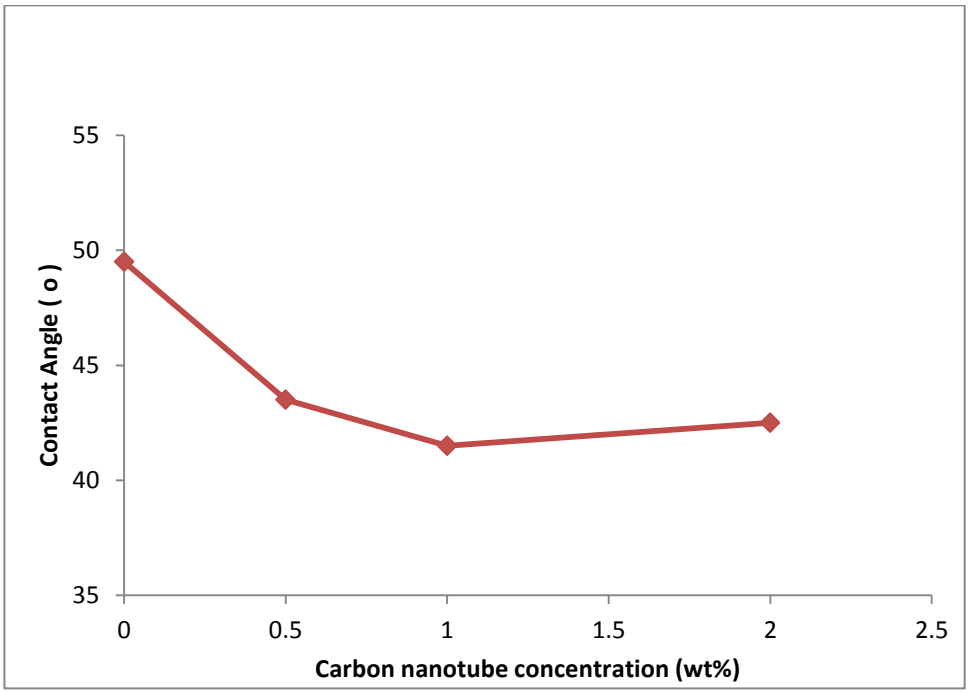


Figure 2.4: Surface contact angle of the hydroxyl functionalized CNTs/ polyacylonitrile membrane (Majeed et al., 2012)

2.5 Methods of measuring contact angle

Several methods are reported in the literature for measuring contact angles depending on the nature of particles, particle size, fluid interfaces (Maestro et al., 2014), surface roughness (Russell, 2009), and chemical heterogeneity (Pegoretti, 2008). The methods include but are not limited to static sessile drop, dynamic sessile drop, Wilhelmy plate (Shang et al., 2008) and vibration-induced equilibrium contact angle measurements (Pegoretti, 2008). However, there are two principle methods available viz: Wilhelmy plate and Goniometry.

2.5.1 Wilhelmy Plate

The Wilhelmy plate technique has been in use for over a century (Wilhelmy, 1863) and it is particularly suitable for measuring a contact angle on substances that have a high surface energy which will yield small contact angles (Chawla et al. 1994). The Wilhelmy plate method comprises of a thin plate, which is vertically submerged into a liquid interface. A force F, which corresponds to interfacial tension σ at a contact angle θ, will act on the plate as shown in Figure 2.5.

The Wilhelmy equation is written as Equation (2.4):

$$\sigma = \frac{F}{L.\cos\theta} \tag{2.4}$$

The contact angle can then be calculated by re-arranging Equation (2.4) to yield Equation (2.5):

$$\theta = \cos^{-1}\left(\frac{F}{L.\sigma}\right) \tag{2.5}$$

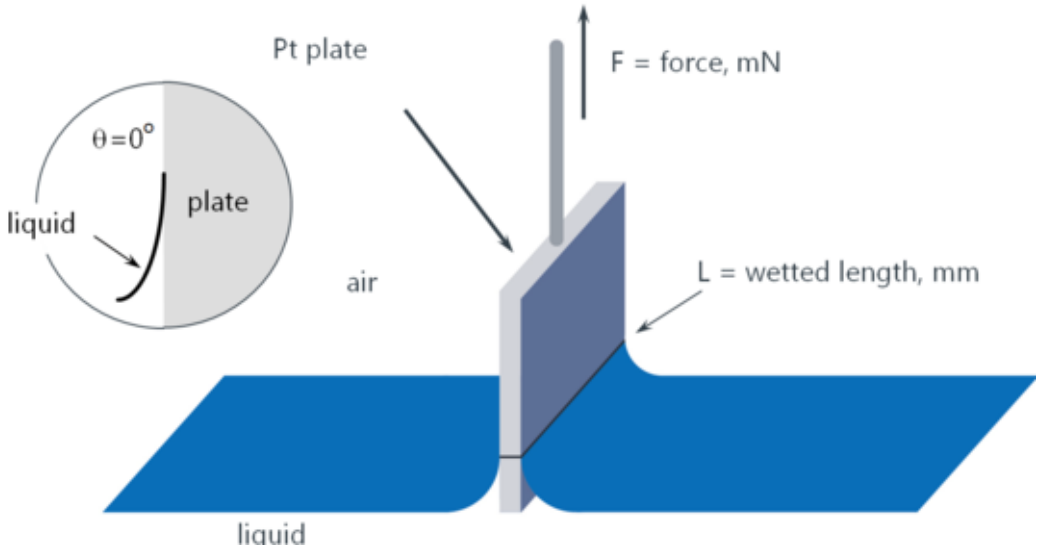


Figure 2.5: Schematic diagram of the Wilhelmy plate method (Kruss, 2014)

2.5.2 Goniometry

In goniometry, a profile image of a back-lit drop is used to obtain contact angles (Ahmed et al., 2014). The contact angle can be measured by direct inspection using optical goniometer or by computerized image processor (Krishnan et al., 2005). While the computerized image processing has significantly decreased labour and bias of goniometry method, it is imperative that the following analytical details (which can be easily neglected during goniometric technique) be given great attention to reduce observer error.

It is important to ascertain a correct contact line which is the intersection between a liquid-vapour interface and a solid surface. Also, the point of contact must be carefully selected. These two details entail that the observer must be looking down on

the drop at a slight angle above the contact line which will reduce the accuracy of the contact angle (Malgarinos et al., 2014).

2.6 Mathematical models for contact angle measurement

2.6.1 Laplace-Young model

Generally, the Laplace-Young equation can be expressed as shown in Equation (2.6) with R_1 and R_2 being the primary radii of curvature, where σ is the surface tension (Bortolotti et al., 2009). The pressure term is divided into two separate components; ΔP_g and ΔP_c. Where ΔP_g is the change in hydrostatic pressure and ΔP_c is the change in pressure due to the curvature of the drop.

$$\left(\frac{1}{R_1} + \frac{1}{R_2}\right)\sigma = \Delta P_g + \Delta P_c \qquad (2.6)$$

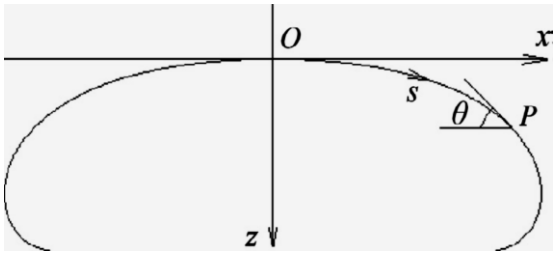


Figure 2.6: Coordinate system for an axisymmetric drop, (Li et al., 1992)

The hydrostatic pressure drop from the apex of the drop in Figure 2.6 is expressed as Equation (2.7):

$$\Delta P_g = \rho g z \qquad (2.7)$$

At the apex of the drop with boundary conditions $\Delta P_g = 0$ and for an axisymmetric drop, $R_1 = R_2 = b$. Thus, the Laplace-Young equation at z = 0 reduces to Equation (2.8):

$$\frac{2\sigma}{b} = \Delta P_c \qquad (2.8)$$

Therefore at any z, the pressure balance can be expressed as Equation (2.9):

$$\left(\frac{1}{R_1} + \frac{1}{R_2}\right)\sigma = \frac{2\sigma}{b} + \rho g z \qquad (2.9)$$

According to Adamson (1990), the local curvature, $\frac{1}{R_1} + \frac{1}{R_2}$, can be expressed in spherical coordinates by recognizing that

$$\frac{1}{R_1} = \frac{d\theta}{ds} \tag{2.10}$$

$$\frac{1}{R_2} = \frac{\sin\theta}{x} \tag{2.11}$$

Equation (2.9) is transformed to Equation (2.12):

$$\frac{d\theta}{ds} = \frac{2}{b} + \frac{\rho g z}{\sigma} - \frac{\sin\theta}{x} \tag{2.12}$$

where $d\theta/ds$ is the radius of curvature, R_1, in spherical coordinates, $2/b$ is the apex curvature term, $\rho g z/\sigma$ relates gravitational effects to capillary effects, $\sin\theta/x$ is the radius of curvature, R_2, in spherical coordinates.

The last step is to write Equation (2.12) as dimensionless coordinates using the ratio of physical properties of the fluid defined as c,

$$c = \frac{\rho g}{\sigma} = \frac{1}{L^2} \tag{2.13}$$

The dimensionless coordinates and apex curvature are defined as

$$X = x c^{\frac{1}{2}} \tag{2.14}$$

$$Z = z c^{\frac{1}{2}} \tag{2.15}$$

$$S = s c^{\frac{1}{2}} \tag{2.16}$$

$$B = b c^{\frac{1}{2}} \tag{2.17}$$

Relating this non-dimensionalization to Equation (2.12) and adding two geometric relationships results in a set of first order ordinary differential equations whose solution fully defines a drop profile,

$$\frac{d\theta}{ds} = \frac{2}{B} + Z - \frac{\sin\theta}{X} \tag{2.18}$$

$$\frac{dX}{dS} = \cos\theta \tag{2.19}$$

$$\frac{dZ}{dS} = \sin\theta \tag{2.20}$$

2.6.2 Hough transformation algorithm

Hough transform was first introduced in 1962 (Hough, 1962) and first used to find lines in images in 1972 (Duda and Hart, 1972). There are two parts to the algorithm: the edge extraction and the Hough transform.

If the line equation corresponding to the solid surface is given as Equation (2.21):

$$ax + by + c = 0 \tag{2.21}$$

and equation of the circle corresponding to the drop edge is given as Equation (2.22):

$$(x - X_o)^2 + (y - Y_o)^2 = R^2 \tag{2.22}$$

Then, the distance from centre of the circle to the line is expressed as Equation (2.23):

$$h = \frac{aX_o + bY_o + c}{\sqrt{a^2 + b^2}} \tag{2.23}$$

The static contact angle in degree is given by Equation (2.24):

$$\theta = 90 - \frac{180a \sin\left(\frac{h}{R}\right)}{\pi} \tag{2.24}$$

2.6.3 Shikhmurzaev's model

Shikhmurzaev (1994) and Shikhmurzaev (2008) described the dependence of dynamic contact angle on the contact line velocity. The model was obtained using methods of non-equilibrium thermodynamics and surface hydrodynamics. To express the model: θ_d represents the dynamic contact angle and θ_e represents static equilibrium value whereby, the model is given as Equation (2.25):

$$\cos\theta_d = \cos\theta_e - \frac{2u(a_1 + a_2 u_o)}{(1 - a_2)[(a_1 + u^2) + u]} \tag{2.25}$$

Where

$$u = a_3 \frac{\mu v}{\sigma}$$

$$u_o = \frac{\sin\theta_d - \theta_d \cos\theta_d}{\sin\theta_d \cos\theta_d - \theta_d}$$

$$a_1 = 1 + (1 - a_2)(\cos\theta_e - a_4)$$

$$a_2 = 0.54, \qquad a_3 = 12.5, \qquad a_4 = 0.07$$

a_1, a_2, a_3 and a_4 are some phenomenological constants.

CHAPTER THREE

MODELLING PROCEDURE

3.1 Introduction

CNTs have been proven to improve hydrophilicity of a polysulfone membrane (Maphutha et al., 2013; Kim et al., 2007; Yin et al., 2013). However, the mathematical relationship between these two variables has not been established. Symbolic regression model is used to predict correlations between the CNT concentration and the contact angle of the nanocomposite membrane using Eureqa^{TM} (desktop version 0.99.9) software. Symbolic regression is a regression analysis method which investigates the relationship among a given dataset and presents mathematical expressions to obtain the model that best fits the dataset (based on precision as well as ease) (Koza, 1992).

This is different from conventional linear and non-linear regression techniques which fit parameters to an equation of an exact form (Sarradj and Geyer, 2014). Symbolic regression finds not only the parameters but the form of the equations at the same time (Koza, 1992). Symbolic regression also known as symbolic function identification, searches for numerous symbolic expressions of functions which fit the given set of data. The chore of regression in general is to find the variables in the data which are linked to the changes in the significant control variables, to articulate these relationships in mathematical models, and then evaluate the precision and simplicity of the designed models (Schmidt and Lipson, 2009). Figure 3.1 shows the stages of the model development.

3.2 Problem Definition

3.2.2 Model objective

The purpose of the model is to predict the relationship between two variables namely: CNT concentration and hydrophilicity of a nanocomposite membrane.

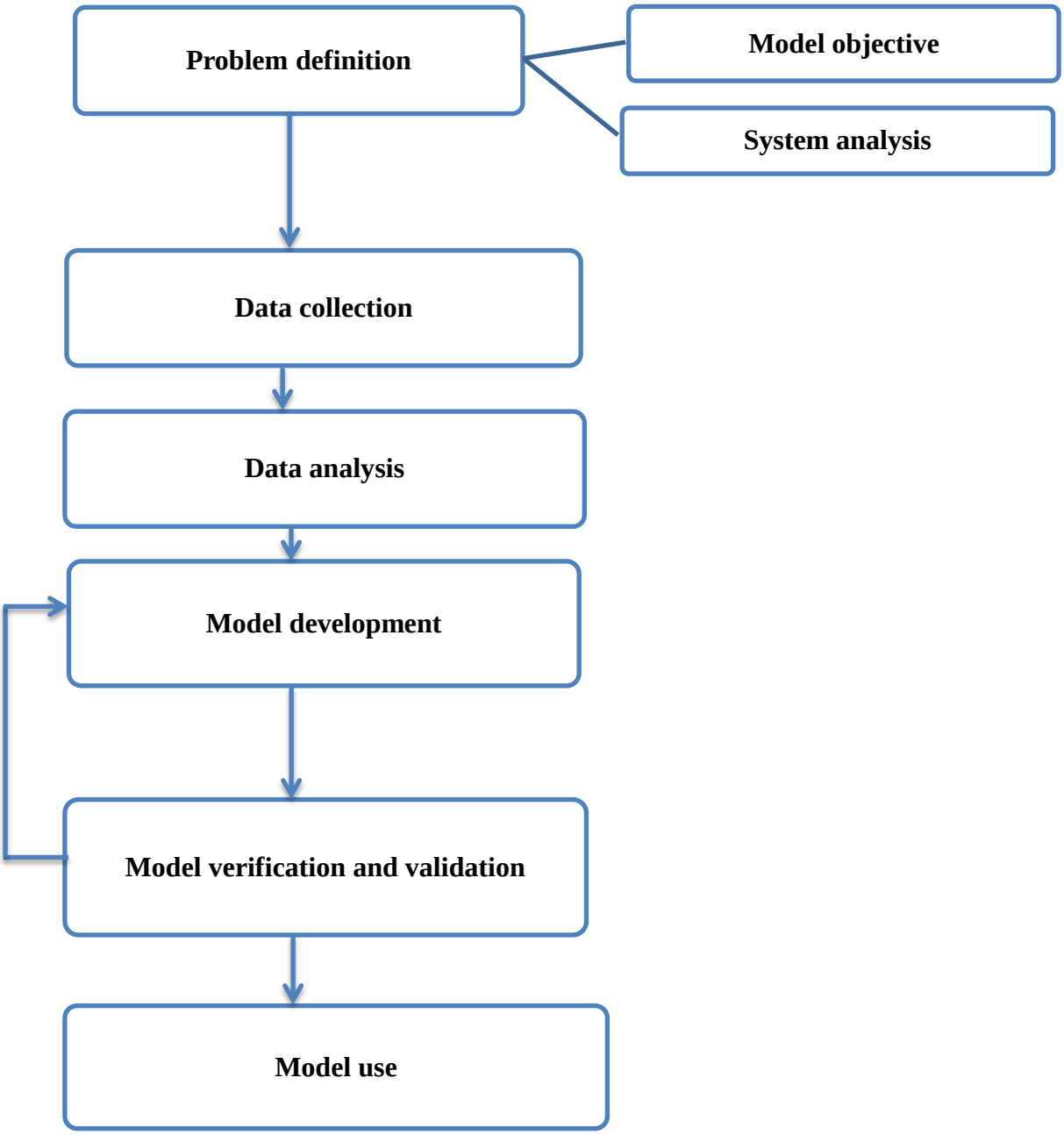


Figure 3.1: Schematic diagram of route through the stages of model development

3.2.3 System Analysis

Hydrophilicity of a nanocomposite membrane is measured by its contact angle. If the contact angle is less than 90^o the membrane is said to be hydrophilic but if the contact angle is greater than 90^o, it is hydrophobic. Also, the more hydrophilic a membrane is the greater the flux rate and oil rejection through the membrane.

The following conditions were imposed on the model:

1. The CNT is functionalized
2. The polymeric membrane is polysulfone membrane

CNT concentration was taken as an independent variable represented by *(x)* whilst contact angle was taken as a dependent variable represented by *(y)*. The mathematical function was represented by Equation (3.1):

$$y = f(x) \tag{3.1}$$

3.3 Data Collection

Previously synthesized functionalized CNT-infused polysulfone membranes within Nanotechnology Research Group in the University of the Witwatersrand, Johannesburg at different CNT concentration were used to determine experimental relationship between CNT concentration and hydrophilicity. A Sessile drop experiment was performed using a Goniometer to determine the water contact angles on the membrane surface at CNT concentration of 0%; 0.04%; 0.08%; 0.1%; 0.2%; 0.3% and 0.4 wt%. Four different readings were taken at each CNT concentration as shown in Table 3.1.

3.4 Data Analysis

The collected data was investigated (based on the system analysis in section 3.2.3) to identify errors in the data. The experimental data showed no inconsistency and is in agreement with the system analysis theory. For every data set at specific CNT concentration, absolute deviation from the mean was calculated, using the Equation (3.2):

$$mean\ Absolute\ deviation\ (MAD) = |y - \mu| \quad (3.2)$$

y = Contact angle at specific CNT concentration

μ = mean of y values for every data set

The mean absolute deviation of the data point is acceptable for the model development as shown in Appendix A. All twenty eight experimental data points were therefore used for the modelling (Table 3.1). Detailed description of the model development is presented in Appendix B.

Table 3.1: Experimental data used for the model development

CNTs concentration (wt%)	**Contact angle (^{o})**			
0	38.33	38.30	38.33	38.31
0.04	35.46	35.43	35.44	35.46
0.08	34.32	34.30	34.32	34.33
0.1	33.88	33.86	33.88	33.88
0.2	32.48	32.44	32.48	32.46
0.3	27.22	27.19	27.24	27.22
0.4	22.52	22.50	22.52	22.52

3.5 Model Verification and Validation

Model verification has to do with developing the model right. This is established by several tests performed to confirm that the model has been developed as intended and that the input data and logical structure of the model have been correctly interpreted. Model validation has to do with developing the right model. This is established by an interactive process of comparing prediction data to experimental data to ensure model accuracy (Paez, 2009).

Based on selected criteria for Eureqa^{TM} as explained in Appendix B, seven possible model equations were returned by Eureqa^{TM}. In other to select the best model, the complexity-to-accuracy Pareto of each model was examined and then was subjected to verification. To verify the models, error metrics of each model was studied to ensure that the input data and logical structure of the model has been correctly

interpreted. Error metrics considered include; mean absolute error, mean square error, R^2 goodness of fit, correlation coefficient, rank correlation, maximum error, median error, inter-quartile absolute error, sign difference error and hybrid correlation error. The detailed error metrics report generated for each model by Eureqa^{TM} is shown in Appendix C.

Additionally, a sensitivity test was performed on the models to see the relative impact within each model that a variable has on the target variable. Given the model function as:

$$y = f(x)$$

The influence metrics of x on y are defined as follows:

Sensitivity: $\overline{\left|\frac{\partial y}{\partial x}\right|} . \frac{\sigma(x)}{\sigma(y)}$ evaluated at all input data points.

% Positive: The percent of data points where $\frac{\partial y}{\partial x} > 0$

% Negative: The percent of data points where $\frac{\partial y}{\partial x} < 0$

Positive magnitude: $\overline{\left|\frac{\partial y}{\partial x}\right|} . \frac{\sigma(x)}{\sigma(y)}$ at all points where $\frac{\partial y}{\partial x} > 0$

Negative magnitude: $\overline{\left|\frac{\partial y}{\partial x}\right|} . \frac{\sigma(x)}{\sigma(y)}$ at all points where $\frac{\partial y}{\partial x} < 0$

The detailed sensitivity report and explanation of terms are shown in Appendix D.

To validate the model, the same data that was used to develop the model was not used in validating the model; otherwise one might think that the model is more accurate than it really is. A new set of experimental data (Qui et al., 2009), outside the region of data space used for the model development was used to validate the model. However, the model underlying assumptions were not changed, i.e. the CNT is functionalized and the polymeric membrane is polysulfone membrane.

The model output and the new experimental data were tested using standard deviation, σ and percentage absolute average relative error, %AARE, to determine the model adequacy using Equations (3.3 – 3.6) (Ahmed, et al., 2014).

$$RE_i = \frac{\theta_i^m - \theta_i^E}{\theta_i^E} \quad (3.3)$$

$$ARE = \frac{1}{N}\sum_{i=1}^{N} RE_i \quad (3.4)$$

$$\sigma = \sqrt{\frac{1}{N}\sum(RE_i - ARE)^2} \quad (3.5)$$

$$\%AARE = \frac{100}{N}\sum_{i=1}^{N}\left|\frac{\theta_i^m - \theta_i^E}{\theta_i^E}\right| \quad (3.6)$$

Where,

RE = Relative error

ARE = Average relative error

θ_i^m = Model contact angle

θ_i^E = Experimental contact angle

N = Number of data points.

CHAPTER FOUR

RESULTS AND DISCUSSION

4.1 Results

The developed model is written as Equation (4.1):

$$\theta = \theta_p + 3361.94C^4 + 771.33C^2 - 94.26C - 2932.29C^3 \quad (4.1)$$

Where:

θ = contact angle of functionalized CNT infused polysulfone membrane

θ_p = contact angle of plain polysulfone membrane

C = concentration of functionalized CNTs added to polysulfone membrane

Eureqa™ generated error metrics that are used to verify Equation (4.1) is shown in Table 4.1 while the complexity-to-accuracy Pareto is shown in Figure 4.1.

Table 4.1: Error metrics for the model equation

Description	value
Mean Absolute Error	0.136379
Mean Square Error	0.027921
R^2 Goodness of Fit	0.998875
Correlation Coefficient	0.999482
Rank Correlation	0.990148
Maximum Error	0.331584
Logarithmic Error	0.027084
Median Error	0.097866
Inter-quartile Absolute Error	0.126569
Signed Difference Error	-0.04635
Hybrid Correlation Error	0.029049

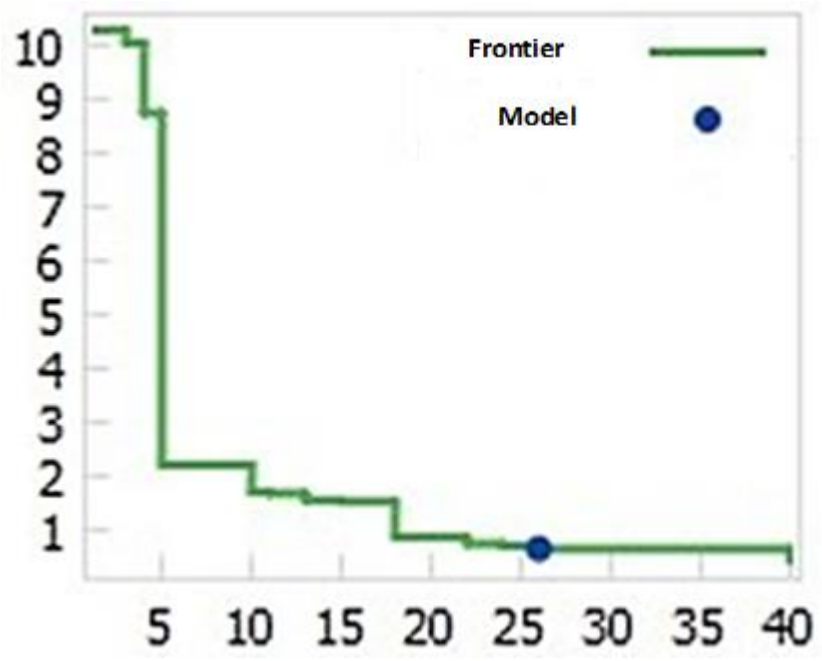


Figure 4.1: complexity-to-accuracy Pareto of the selected model

The model output and fit against the experimental data used for the model development is shown in Table 4.2 and Figure 4.2. The average experimental contact angles at different CNT concentration were taken into consideration and the values of CNT concentration were substituted into Equation (4.1) to generate the model contact angle.

Table 4.2: Model output versus experimental data

CNT concentration (wt %)	Experimental contact angle	Model contact angle
0.00	38.32	38.32
0.04	35.45	35.60
0.08	34.32	34.35
0.10	33.88	34.01
0.20	32.47	32.24
0.30	27.22	27.52
0.40	22.52	22.43

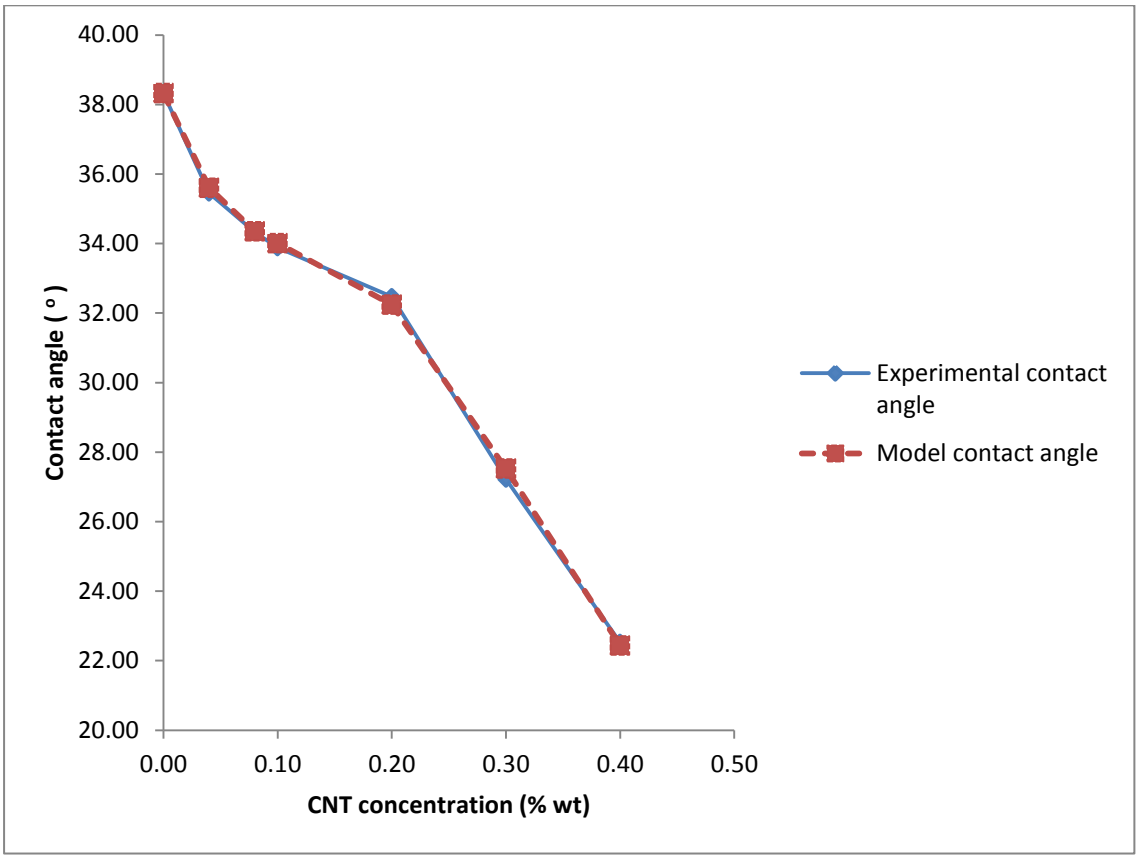


Figure 4.2: Model fit against the experimental data.

The model output and fit against the experimental data used for the model validation are shown in Figure 4.3.

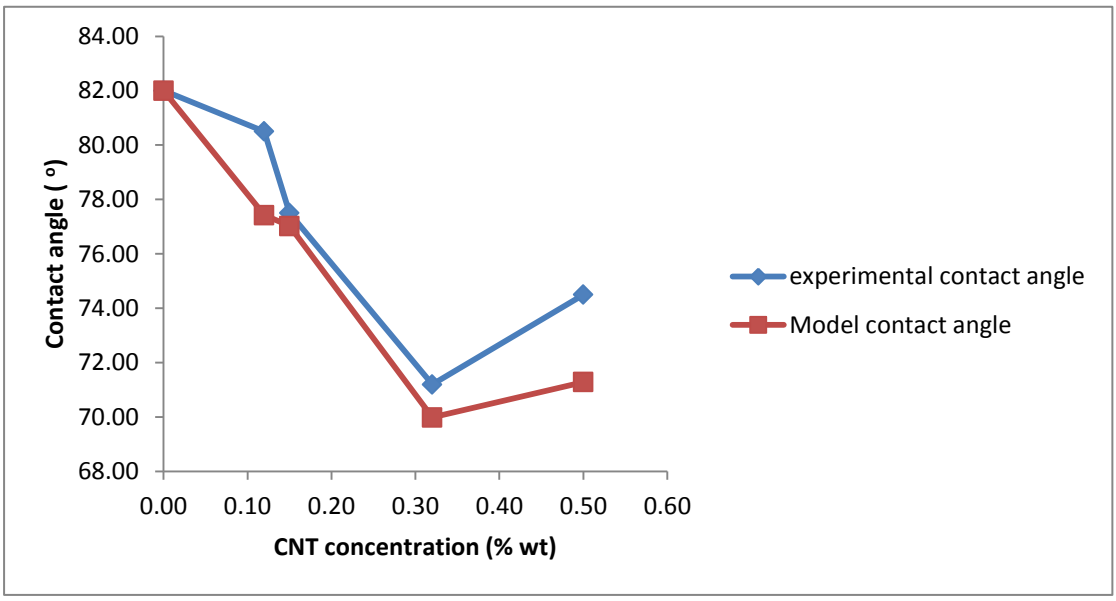


Figure 4.3: Model fit against the validating experimental data

The parameters for calculating standard deviation, σ and absolute average relative error, AARE, for model output and the new experimental data testing, are shown in Table 4.3.

Table 4.3: Standard deviation and AARE calculation parameters for model validation

$\boldsymbol{\theta_i^m}$	$\boldsymbol{\theta_i^E}$	$\boldsymbol{RE_i = \frac{\theta_i^m - \theta_i^E}{\theta_i^E}}$	$\boldsymbol{(RE_i - ARE)^2}$	$\boldsymbol{\left\lvert\frac{\theta_i^m - \theta_i^E}{\theta_i^E}\right\rvert}$
82.00	82.00	0.000000	0.000437	0.000000
77.43	80.50	-0.038185	0.000299	0.038185
77.02	77.50	-0.006175	0.000217	0.006175
69.99	71.20	-0.017020	0.000015	0.017020
71.29	74.50	-0.043121	0.000494	0.043121

$$ARE = \frac{1}{N}\sum_{i=1}^{N} RE_i \quad = \quad -0.0209$$

$$\sigma = \sqrt{\frac{1}{N}\sum (RE_i - ARE)^2} \quad = \quad 0.017$$

$$\%AARE = \frac{100}{N}\sum_{i=1}^{N}\left|\frac{\theta_i^m - \theta_i^E}{\theta_i^E}\right| \quad = \quad 2.09\%$$

4.2 Discussion

In Table 4.2, the experimental contact angle of plain polysulfone membrane was 38.32^o which confirmed that the plain membrane was hydrophilic. The contact angle was that low because chloroform was used as polysulfone solvent. For a dimethyformamide (DMF) solvent, the membrane contact angle was 82^o as shown in the validating experimental data (Table 4.3) because DMF is more hydrophobic that chloroform (Qiu et al., 2009). An increase in CNT concentration of the synthesized membrane from 0% to 0.4% decreased the experimental contact angle from 38.32^o to

22.52^{o}. This showed that the hydrophilicity of the membrane was enhanced by the addition of functionalized CNTs.

In the developed model Equation (4.1), θ_p was introduced into the model equation to factor in the initial hydrophilicity of the plain polysulfone membrane which is dependent on the base solvent of the polysulfone membrane. Therefore, for the model to effectively predict the contact angle of functionalized CNT infused polysulfone membrane, the contact angle of the plain polysulfone membrane must be provided. The positive signs in the model Equation (4.1) represent positive sensitivity of the model i.e. an increase in the value of this variable will increase the value of the target variable. The negative signs are responsible for negative sensitivity of the model, that is, an increase in the value of this variable will decrease the value of the target variable.

Appendix D shows the sensitivity report of all the models and the selected model has sensitivity of 1.1322. This means that the relative impact within the model that CNT concentration has on the contact angle was 1.1322. For an increase in CNT concentration from 0% to 0.4%, the percentage positive sensitivity of the model was 0% i.e. an increase in CNT concentration from 0% to 0.4% will not increase the contact angle of the synthesized membrane. While the percentage negative sensitivity of the model within the same CNT concentration range was 100% i.e. an increase in CNT concentration from 0% to 0.4% will lead to decrease in the contact angle of the synthesized membrane. Hence, the hydrophilicity of the functionalized CNT-infused polysulfone membrane will be enhanced within 0% - 0.4% wt CNT.

In the work of Shah and Murthy (2013), the lowest pore size obtained with amide functionalized CNT/PSF membrane was at the CNT concentration of 0.5 wt%. No further reduction in pore size was achieved as more of the CNTs were added to the membrane. Hence, the enhancement of hydrophilicity of the functionalized CNT/PSF membrane was achieved within 0 - 0.5 wt% CNT.

One of the factors to consider when developing a model is the trade-off between complexity (size) and accuracy (fit) of the model. Figure 4.1 shows the plot of complexity against accuracy of the selected model. At a complexity of 26, the accuracy of the model is at its optimum. Further increase in size of the model will

only increase the processing time of the model without significantly improving its accuracy. Therefore the model with complexity-to-accuracy Pareto of 26 is described as the best model of the seven models returned by Eureqa^{TM}. The complexity-to-accuracy Pareto of the other models is shown in Appendix E.

Table 4.1 shows the error metrics of the developed model output against the input data. The signed difference error which is a summary of how well the model contact angle matches the input contact angle was -0.046. Hybrid correlation error which is the linear combination between correlation and mean absolute error was 0.029. R^2 goodness of fit which is a measure of how well the regression line approximates the input data was 99.89%. The results confirmed that the input data and the logical structure of the model have been correctly interpreted. The error metrics for other non-selected models are shown in Appendix C.

However, statistical plausibility of the model output against the input data is not enough to validate the model. The model needs to be tested with a new set of input data outside the region of data space used for the model development (Ferrentino et al., 2014). The input data for the model development was obtained from CNTs functionalized by 35% nitric acid solution and blended with polysulfone membrane with chloroform as its base solvent (Maphutha et al., 2013). While the input data for model testing was obtained from CNTs functionalized by 5-isocyanato-isophthaloyl chloride (ICIC) blended with polysulfone membrane with DMF as its base solvent (Qiu et al., 2009). Figure 4.3 shows the model output against the validating input data.

To test the model adequacy, standard deviation, σ which is a measure of amount of variation from the expected outcome and percentage absolute average relative error, %AARE were used. The standard deviation of the model output against the validating experimental input was 0.017. This showed that the model contact angles tend to be very close to the validating experimental contact angles. As %AARE was 2.09%, this confirmed near to perfect fit between the model contact angle and the validating experimental contact angle.

CHAPTER FIVE

CONCLUSION AND RECOMMENDATIONS

5.1 Conclusion

Membrane technology has been commonly used worldwide for the removal of suspended solids especially in water-oil separation. However, fouling is still a major problem limiting the wider application of membrane operations. This is because the existing polymeric membrane materials seem to have reached a maximum level of compromise between permeability and selectivity.

This study showed that one of the best ways of improving the efficiency of polymeric membrane and modifying its surface characteristic is by adding functionalized CNTs. The hydrophilicity of the blend membrane improved with an increase in concentrations of functionalized CNTs, which causes an increase in water flux rate and improved fouling resistance because most fouling agents are naturally hydrophobic.

However, when CNT concentration exceeded ~0.5% (wt), contact angle of the blend membrane increased which showed a decrease in hydrophilicity. This could be due to high steric hindrance and electrostatic interactions between modified CNTs and polymeric membrane or agglomeration of modified CNTs in the polymer matrix. The high concentration of CNTs in the nanocomposite could decrease the porosity of the nanocomposite.

The accuracy of methods of contact angle measurement (hydrophilicity test) is largely dependent on smoothness of the membrane surface, nature of particles, particle size, fluid interfaces and chemical heterogeneity. In this work, a mathematical model that can effectively predict the contact angle of functionalized CNT-infused polysulfone membrane for water-oil treatment was developed (without dependence on imaging of the contact line). The developed model equation is written as:

$$\theta = \theta_p + 3361.94C^4 + 771.33C^2 - 94.26C - 2932.29C^3$$

Hydrophilicity tests were performed on functionalized CNT infused polysulfone membrane by sessile drop method using Goniometer at CNT concentration of 0%;

0.04%; 0.08%; 0.1%; 0.2%; 0.3% and 0.4% wt. The result showed that the contact angle of the synthesized membrane decreased from 38.32^{o} to 22.52^{o} as the CNT concentration was increased from 0% to 0.4%. This confirmed that the hydrophilicity of the membrane was enhanced by the addition of functionalized CNT.

A symbolic regression model was used to predict correlations between the CNT concentration and the contact angle of the nanocomposite membrane using Eureqa™ (desktop version 0.99.9) software. Seven possible model equations were returned by Eureqa™. In order to select the best model, the complexity-to-accuracy Pareto of each model was examined and subjected to verification. The models were verified using error metrics generated from Eureqa™ so as to ensure that the input data and logical structure of the model have been correctly interpreted. Error metrics considered include; mean absolute error, mean square error, R^2 goodness of fit, correlation coefficient, rank correlation, maximum error, median error, inter-quartile absolute error, sign difference error and hybrid correlation error. Also, a sensitivity test was performed on the models to gauge the relative impact within each model that a variable has on the target variable.

The selected model was adjusted based on the underlying model assumptions. The final model was tested for adequacy by means of standard deviation, σ and percentage absolute average relative error, %AARE using new set of experimental data outside the region of data space used for the model development. The results showed that standard deviation, σ and %AARE of the model output against the validating experimental data are 0.017 and 2.09% respectively. This indicated that the model is adequate to predict hydrophilicity of functionalized CNT-infused PSF membrane.

5.2 Recommendations

Further research should be focused on developing a mathematical model to determine:

- The hydrophilicity of nanocomposites with respect to the concentration of other modifying materials (e.g zeolite) added to membranes without restriction to CNTs.
- The hydrophilicity of nanocomposites with respect to the CNT concentration for different types of membrane such as polyethersulfone.

REFERENCES

Adamson, A. W. (1990) Physical Chemistry of Surfaces, *John Wiley and Sons*.

Ahmed, G., Sellier, M., Jermy, M. and Taylor, M. (2014) Modelling the effects of contact angle hysteresis on the sliding of droplets down inclined surfaces, *European Journal of Mechanics B/Fluids*, vol. 48, pp. 218–230.

Baek, Y., Kang, J., Theato, P., and Yoon, J. (2012) Measuring hydrophilicity of RO membranes by contact angles via sessile drop and captive bubble method: A comparative study, *Desalination*, vol. 303, pp. 23–28.

Bekou, S. and Mattia, D. (2011) Wetting of nanotubes, *Current Opinion in Colloid & Interface Science*, vol. 16, pp. 259–265.

Bortolotti, M., Brugnara, M., Volpe, C. D. and Siboni, S. (2009) Numerical models for the evaluation of the contact angle from axisymmetric drop profiles: A statistical comparison, *Journal of Colloid and Interface Science*, vol. 336, pp. 285–297.

Cai, W., Pacheco-Vega, A., Sen, M. and Yang, K. T. (2006) Heat transfer correlations by symbolic regression, *International Journal of Heat and Mass Transfer*, vol. 49, pp. 4352–4359.

Celik, E., Park, H. and Choi, H. (2011) Carbon nanotube blended polyethersulfone membranes for fouling control in water treatment, *Water Research*, vol. 45, pp. 274-282.

Chawla, A., Buckton, G., Taylor, K. M. G., Newton, J. M. and Johnson, M. C. R. (1994) Wilhelmy plate contact angle data on powder compacts: considerations of plate perimeter, *European Journal of Pharmaceutical Sciences*, vol. 2, pp. 253-258.

Chen, L., Xie, H., Li, Y. and Yu, W. (2008) Surface Chemical Modification of Multi-walled Carbon Nanotubes by a Wet-Mechanochemical Reaction, *Journal of Nanomaterials*, Article ID 783981.

Chini, S. F. and Amirfazli, A. (2011) A method for measuring contact angle of asymmetric and symmetric drops, *Colloids and surface A: physicochemical and engineering aspects*, vol. 388, pp 29-37.

Chowdhury, S.C., Haque, B. Z., Okabe, T. and Gillespie, J. W. (2012) Modelling the effect of statistical variations in length and diameter of randomly oriented CNTs on the properties of CNT reinforced nanocomposites, *Composites: Part B*, vol. 43, pp. 1756–1762.

Das, A.K. and Das, P.K. (2010) Equilibrium shape and contact angle of sessile drops of different volumes—Computation by SPH and its further improvement by DI, *Chemical Engineering Science*, vol. 65, pp. 4027–4037.

Davidson, J.W. and Savic, D.A. (2003) Walters G.A., Symbolic and numerical regression: experiments and applications, *Information Sciences*, vol. 150 pp. 95–117.

De Lannoy, C.-F., Soyer, E. and Wiesner, M. R. (2013) Optimizing carbon nanotube-reinforced polysulfone ultrafiltration membranes through carboxylic acid functionalization, *Journal of Membrane Science*, vol. 447, pp. 395–402.

Du, J.-H., Bai, J. and Cheng, H.-M. (2007) The present status and key problems of carbon nanotube based polymer composites, *Polymer Letters*, vol. 1, No.5, pp. 253–273.

Duda, R. O. and Hart, P. E. (1972) Use of the Hough Transformation to detect lines and curves in pictures, *Association for Computing Machinery, Inc.*

Dyachkova, T. P. (2013) Some aspects of functionalization and modification of carbon nanomaterials**,** *Nanosystems: Physics, Chemistry, Mathematics*, vol. 4, pp. 605–621.

Ferrentino, G., Calliari, N., Bertucco, A. and Spilimbergo, S. (2014) Validation of a mathematical model for predicting high pressure carbon dioxide inactivation kinetics of Escherichia coli spiked on fresh cut carrot, *The Journal of Supercritical Fluids*, vol. 85, pp. 17– 23.

Hashemifard, S. A., Ismail, A. F. and Matsuura, T. (2010) Prediction of gas permeability in mixed matrix membranes using theoretical models, *Journal of Membrane Science*, vol. 347, pp. 53–61.

Hirsch, A. (2002) Functionalization of singe-walled carbon nanotube. *Angewandte Chemie International*, vol. 41, pp 1853-9.

Hough, P.V.C. (1962) Method and means for recognizing complex patterns. *U.S. Patent* 3,069,654, Dec. 18, 1962.

Iijima, S. (1991) Helical microtubules of graphitic carbon, *Nature*, vol. 354, pp. 56-58.

Inam, F. and Peijs, T. (2007) Re-agglomeration of carbon nanotubes in two-part epoxy system; influence of the concentration. In: *5th International Bhurbhan Conference on Applied Science and Technology (IBCAST 2007)*, 8-11 January 2007, Pakistan.

Ismail, A.F., Goh, P. S., Sanip, S. M. and Aziz, M. (2009) Transport and separation properties of carbon nanotube-mixed matrix membrane, *Separation and Purification Technology*, vol. 70, pp. 12–26.

Jogi, B. F., Sawant, M., Kulkarni, M. and Brahmankar, P. K. (2012) Dispersion and Performance Properties of Carbon Nanotubes (CNTs) Based Polymer Composites: A Review, *Journal of Encapsulation and Adsorption Sciences*, vol. 2, pp. 69-78.

Kim, S., Chen, L., Johnson, J. K. and Marand, E. (2007) Polysulfone and functionalized carbon nanotube mixed matrix membranes for gas separation: Theory and experiment, *Journal of Membrane Science*, vol. 294, pp. 147–158.

Kirtania, S. and Chakraborty, D. (2012) Multi-scale modelling of carbon nanotube reinforced composites with a fiber break, *Materials and Design*, vol. 35, pp. 498–504.

Koza, J. R. (1992) Genetic Programming: On the Programming of Computers by Means of Natural Selection, *MIT Press*.

Krishnan, A., Liu, Y.-H., Chab, P., Woodward, R., Allara, D. and Vogler, E. A. (2005) An evaluation of methods for contact angle measurement, *Colloids and Surfaces B: Biointerfaces*, vol. 43, pp. 95–98.

Kruss GmbH (2014) Wilhelmy plate method. Available from *http://www.kruss.de/services/education-theory/glossary/wilhelmy-plate-method*. [October 2014].

Kumar, M. and Ulbricht, M. (2014) Low fouling negatively charged hybrid ultrafiltration membranes for protein separation from sulfonated poly(arylene ethersulfone) block copolymer and functionalized multiwalled carbon nanotubes, *Separation and Purification Technology,* vol. 127, pp. 181–191.

Li, D., Cheng, P., and Neumann, A. W. (1992) Contact angle measurement by axisymmetric drop shape analysis (ADSA), *Advances in Colloid and Interface Science,* vol. 39, pp. 347-382.

Lin, T., Bajpa, V. Ji, T. and Dai, L. (2003) Chemistry of carbon nanotubes, *Australian Journal of Chemistry,* vol. 56, pp. 635-651.

Ma, P.-C., Siddiqui, N. A., Marom, G. and Kim, J.-K. (2010) Dispersion and functionalization of carbon nanotubes for polymer-based nanocomposites: A review, *Composites*: Part A vol. 41, pp. 1345–1367.

Maestro, A., Guzman, E., Ortega, F. and Rubio, R. G. (2014) Contact angle of micro- and nanoparticles at fluid interfaces, *Current Opinion in Colloid and Interface Science,* article in press.

Majeed, S., Fierro, D., Buhr, K., Wind, J., Du, B., Boschetti-de-Fierro, A. and Abetz, V. (2012) Multi-walled carbon nanotubes (MWCNTs) mixed polyacrylonitrile (PAN) ultrafiltration membranes, *Journal of Membrane Science,* vol. 403-404, pp. 101-109.

Malgarinos, I., Nikolopoulos, N., Marengo M., Carlo Antonini, C. and Gavaises, M. (2014) VOF simulations of the contact angle dynamics during the drop spreading: Standard models and a new wetting force model, *Advances in Colloid and Interface Science,* article in press.

Maphutha, S., Moothi, K., Meyyappan, M. and Iyuke, S. E. (2013) A carbon nanotube-infused polysulfone membrane with polyvinyl alcohol layer for treating oil-containing waste water, *Scientific Reports*, vol. 3, srep 1509.

Mattia, D., Lee, K. P. and Calabro, F. (2014) Water permeation in carbon nanotube membranes, *Current Opinion in Chemical Engineering*, vol. 4, pp. 32–37.

Naderi, A. (2013) Effect of the method of dispersion on the properties of carbon nanotube and microfibrillar cellulose composite, *Innventia Report*, no. 433.

Ortiz-Arroyo, A., Larachi, F. and Iliuta, I. (2003) Method for inferring contact angle and for correlating static liquid hold-up in packed beds, *Chemical Engineering Science,* vol. 58, pp. 2835 – 2855.

Paez, T. L. (2009) Introduction to Model Validation**,** Proceedings of the IMAC-XXVII February 9-12, 2009 Orlando, Florida USA, *Society for Experimental Mechanics Inc.*

Park, S.-M., Jung, J., Lee, S., Baek, Y., Yoon, J., Seo, D. K. and Kim, Y. H. (2014) Fouling and rejection behavior of carbon nanotube membranes, *Desalination*, vol. 343, pp. 180–186.

Pegoretti, A., Dorigato, A., Brugnara, M. and Penati, A. (2008) Contact angle measurements as a tool to investigate the filler–matrix interactions in polyurethane–clay nanocomposites from blocked prepolymer, *European Polymer Journal*, vol. 44 pp. 1662–1672.

Peponi, L. Tercjak, A., Martin, L., Mondragon, I. and Kenny J. M. (2011) Morphology-properties relationship on nanocomposite films based on poly (styrene-*block*-diene-*block*-styrene) copolymers and silver nanoparticles, *Polymer Letters*, vol.5, no.2, pp. 104–118.

Phan, H.T. Caney, N., Marty, P., Colasson, S. and Gavillet, J. (2010) A model to predict the effect of contact angle on the bubble departure diameter during heterogeneous boiling, *International Communications in Heat and Mass Transfer,* vol. 37, pp. 964–969.

Qiu, S., Wu, L., Pan, X., Zhang, L., Chen, H. and Gao, C. (2009) Preparation and properties of functionalized carbon nanotube/PSF blend ultrafiltration membranes, *Journal of Membrane Science,* vol. 342, pp. 165-172.

Rafiee, R. and Pourazizi, R. (2014) Influence of CNT functionalization on the interphase region between CNT and polymer, *Computational Materials Science*, article in press.

Rahimpour, A., Jahanshahi, M., Khalili, S., Mollahosseini, A., Zirepour, A. and Rajaeian, B. (2012) Novel functionalized carbon nanotubes for improving the surface properties and performance of polyethersulfone (PES) membrane, *Desalination*, vol. 286, pp. 99–107.

Rana, D. and Matsuura, T. (2010) Surface modifications for antifouling membranes, *Chemical reviews*, vol. 110, pp. 2448–2471.

Ranaa, D., Kima, Y., Matsuuraa, T. and Arafat, H. A. (2011) Development of antifouling thin-film-composite membranes for seawater desalination, *Journal of Membrane Science*, vol. 367, pp. 110–118.

Reyes, Y., Paulis, M. and Leiza, J. R. (2010) Modelling the equilibrium morphology of nanodroplets in the presence of nanofillers, *Journal of Colloid and Interface Science*, vol. 352, pp. 359–365.

Russell, S., *Contact Angle Measurement Technique for Rough Surfaces*, Msc Thesis, Michigan Technological University, Michigan, 2009.

Saha, A. A. and Mitra, S.K. (2009) Effect of dynamic contact angle in a volume of fluid (VOF) model for a microfluidic capillary flow, *Journal of Colloid and Interface Science*, vol. 339, pp. 461–480.

Sarradj, E. and Geyer, T. (2014) Symbolic regression modeling of noise generation at porous airfoils, *Journal of Sound and Vibration*, vol. 33, pp. 3189–3202.

Schmidt, M. and Lipson, H. (2009) *Symbolic Regression of Implicit Equations*, In book: Genetic Programming Theory and Practice VII, Publisher: Springer, Editors: Rick L. Riolo, Una-May O'Reilly, Trent McConaghy, pp.73-85.

Shah, P. and Murthy, C. N. (2013) Studies on the porosity control of MWCNT/polysulfone composite membrane and its effect on metal removal, *Journal of Membrane Science*, vol. 437, pp. 90-98.

Shang, J., Flury, M., Harsh, J. B. and Zollars, R. L. (2008) Comparison of different methods to measure contact angles of soil colloids, *Journal of Colloid and Interface Science*, vol. 328, pp. 299–307.

Shikhmurzaev, Y. D. (1994) Mathematical modelling of wetting hydrodynamics, *Fluid Dynamics Research*, vol. 13, pp. 45-64.

Shikhmurzaev, Y. D. (2008a) On Young's (1805) equation and Finn's (2006) 'counterexample', *Physics Letters A*, vol. 372, pp. 704–707.

Shikhmurzaev, Y. D. (2008b) Capillary Flows with Forming Interfaces, *Chapman & Hall/CRC Taylor & Francis group*.

Shimekit, B., Mukhtar, H. and Maitra, S. (2010) Comparison of Predictive Models for Relative Permeability of CO_2 in Matrimid-Carbon Molecular Sieve Mixed Matrix Membrane. *Journal of Applied Sciences,* vol. 10, pp. 1204-1211.

Stalder, A. F., Melchior, T., Müller, M., Sage, D., Blu, T. and Unser, M. (2010) Low-bond axisymmetric drop shape analysis for surface tension and contact angle measurements of sessile drops, *Colloids and Surfaces A: Physicochem. Eng. Aspects,* vol. 364, pp. 72–81.

Tasis, D., Tagmatarichis, N., Bianco, A. and Prato, M. (2006) Chemistry of carbon nanotubes, *Chemical Review,* vol. 106, pp. 1105-1136.

Toth, A. and Laszlo, K. (2012) Water Adsorption by Carbons: Hydrophobicity and Hydrophilicity, *Novel Carbon Adsorbents*, pp. 147-171.

Vafaei, S. and Podowski, M.Z. (2005) Analysis of the relationship between liquid droplet size and contact angle, *Advances in Colloid and Interface Science,* vol. 113, pp. 133–146.

Vatanpour, V., Esmaeili, M. and Farahani, M. H. D. A. (2014) Fouling reduction and retention increment of polyethersulfone nanofiltration membranes embedded by amine-functionalized multi-walled carbon nanotubes, *Journal of Membrane Science*, vol. 466, pp.70–81.

Wang, T., Shen, J.-N., Wu, L.-G. and Bruggen, B. V. (2014) Improvement in the permeation performance of hybrid membranes by the incorporation of functional multi-walled carbon nanotubes, *Journal of Membrane Science,* vol. 466, pp. 338–347.

Wilhelmy, L. (1863) Concerning the dependence of the Capillaritäts - Constante the alcohol of substance and shape of the wetted solid body, *Annalen Der Physik und Chemie*, vol. 119, pp 177.

World Intellectual Property Organization, 2009. High performance mixed matrix membranes incorporating at least two kinds of molecular sieves. Available from *http://www.wipo.int/pctdb/en/*. [June 2014].

Wu, H., Tang, B. and Wu, P. (2010) Novel ultrafiltration membranes prepared from a multi-walled carbon nanotubes/polymer composite, *Journal of Membrane Science*, vol. 362, pp. 374-383.

Xu, Z. (2014) A high accurate static contact angle algorithm based on Hough transformation, *Measurement*, vol. 55, pp. 97–100.

Yakobson, B.I. and Avouris, P. (2001) Mechanical properties of carbon nanotubes, *Topics in applied physics*, vol. 80, pp. 287-327.

Yang, Y. -K., Xie, X. -L. and Mai, Y. -W. (2011) Functionalization of carbon nanotubes for polymer nanocomposites, *Woodhead Publishing Limited, pp. 55-91*.

Yin, J., Zhu, G. and Deng, B. (2013) Multi-walled carbon nanotubes (MWNTs)/polysulfone (PSU) mixed matrix hollow fiber membranes for enhanced water treatment, *Journal of Membrane Science*, vol. 437, pp. 237–248.

Zhang, Y., *Symbolic regression of thermo-physical model using genetic programming*, Msc Thesis, University of South Florida, Tampa, Florida, 2004.

Zhao, X., Ma, J., Wang, Z., Wen, G., Jiang, J., Shi, F. and Sheng, L. (2012) Hyperbranched-polymer functionalized multi-walled carbon nanotubes for poly (vinylidene fluoride) membranes: From dispersion to blended fouling-control membrane, *Desalination*, vol. 303, pp. 29–38.

APPENDIX A

EXPERIMENTAL DATA ANALYSIS

For every data set at specific CNT concentration, absolute deviation from the mean was calculated to determine if there is an inconsistency in the experimental contact angle and if they are in agreement with the system analysis theory, using the Equation (A1):

$$mean\ Absolute\ deviation\ (MAD) = |y - \mu| \quad \text{(A1)}$$

y = Contact angle at specific CNT concentration

μ = mean of y values for every data set

The mean value for each data set was calculated and subtracted from y values. The absolute value was then determined and results shown in Tables A1 – A7.

Table A1: MAD of the experimental contact angle at 0 wt% CNT concentration

Experimental contact angle (°)	**MAD** $\|y - \mu\|$
38.33	0.0125
38.30	0.0175
38.33	0.0125
38.31	0.0075
μ = 38.3175	

Table A2: MAD of the experimental contact angle at 0.04 wt% CNT concentration

Experimental contact angle (°)	**MAD** $\|y - \mu\|$
35.46	0.0125
35.43	0.0175
35.44	0.0075
35.46	0.0125
μ = 35.4475	

Table A3: MAD of the experimental contact angle at 0.08 wt% CNT concentration

Experimental contact angle (°)	**MAD** $\|y - \mu\|$
34.32	0.0025
34.30	0.0175
34.32	0.0025
34.33	0.0125
μ = 34.3175	

Table A4: MAD of the experimental contact angle at 0.10 wt% CNT concentration

Experimental contact angle (^{o})	**MAD** $\|y - \mu\|$
33.88	0.0050
33.86	0.0150
33.88	0.0050
33.88	0.0050
μ **= 33.8750**	

Table A5: MAD of the experimental contact angle at 0.20 wt% CNT concentration

Experimental contact angle (^{o})	**MAD** $\|y - \mu\|$
32.48	0.0150
32.44	0.0250
32.48	0.0150
32.46	0.0050
μ **= 32.4650**	

Table A6: MAD of the experimental contact angle at 0.30 wt% CNT concentration

Experimental contact angle (^{o})	**MAD** $\|y - \mu\|$
27.22	0.0025
27.19	0.0275
27.24	0.0225
27.22	0.0025
μ **= 27.2175**	

Table A7: MAD of the experimental contact angle at 0.4 wt% CNT concentration

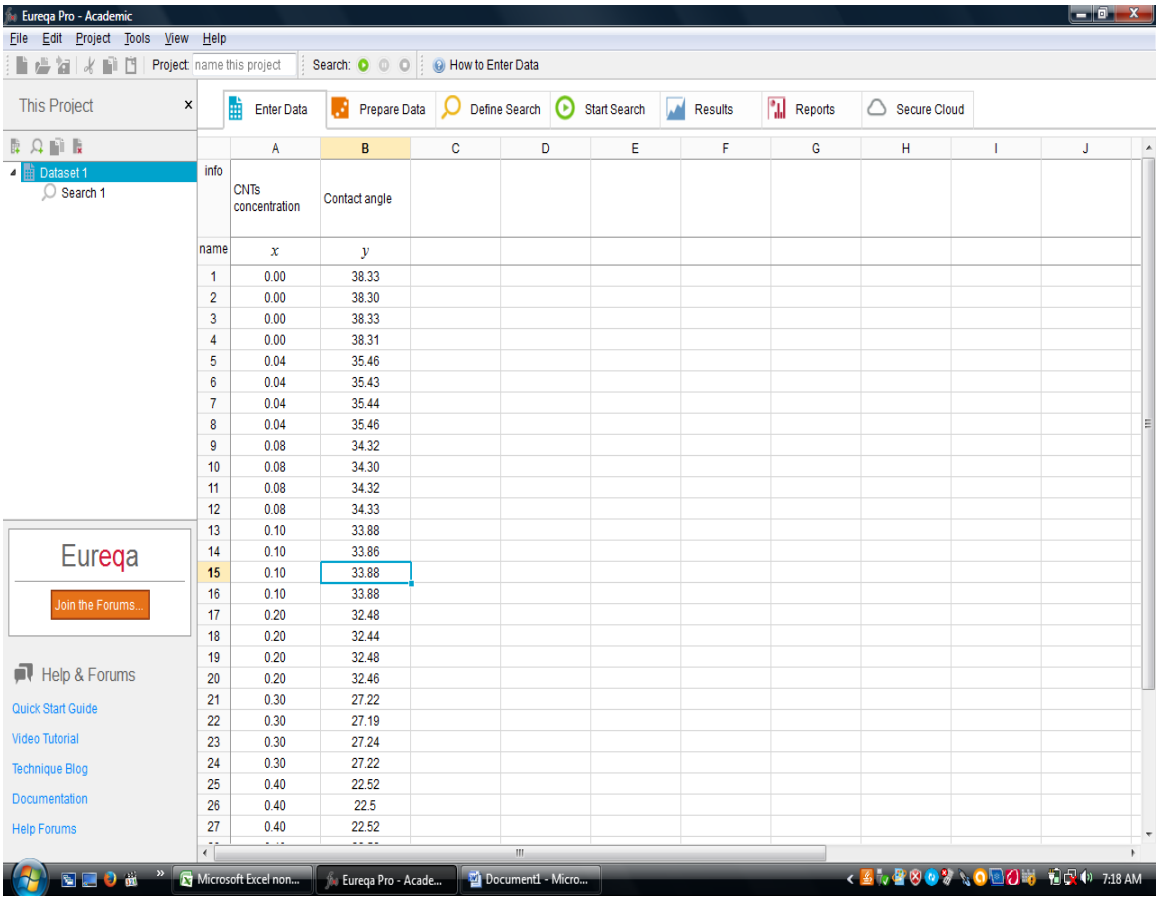
Experimental contact angle (^{o})	**MAD** $\|y - \mu\|$
22.52	0.0050
22.50	0.0150
22.52	0.0050
22.52	0.0050
μ **= 22.5150**	

APPENDIX B

MODEL DEVELOPMENT

This section describes how Eureqa™ was used to obtain initial models which are then subjected to verification and validation to achieve the final model.

The experimental data was input into Eureqa™ spreadsheet-like view, Enter Data tab to replace the default example data variable. The first row labelled "info" is the description of data in the column below. The second row labelled "name" is the name given to the variables. The remaining rows represent a set of measurements which are simultaneous as shown in Figure B1.



	A	B
1	0.00	38.33
2	0.00	38.30
3	0.00	38.33
4	0.00	38.31
5	0.04	35.46
6	0.04	35.43
7	0.04	35.44
8	0.04	35.46
9	0.08	34.32
10	0.08	34.30
11	0.08	34.32
12	0.08	34.33
13	0.10	33.88
14	0.10	33.86
15	0.10	33.88
16	0.10	33.88
17	0.20	32.48
18	0.20	32.44
19	0.20	32.48
20	0.20	32.46
21	0.30	27.22
22	0.30	27.19
23	0.30	27.24
24	0.30	27.22
25	0.40	22.52
26	0.40	22.5
27	0.40	22.52

Figure B1: Screen shot of enter data tab of Eureqa™

Figures B2 and B3 show the Prepare Data tab for x and y variables. This tab offers pre-processing options for the x and y data values which include smooth data points, handle missing values, remove outliers, normalize scale and offset and filter data. The first option is smooth data points, which can greatly improve both the speed of search and the likelihood of finding accurate solutions. Independent variables to smooth were selected and automatic smoothness was chosen. The Eureqa™ then gave the best smooth as determined by generalized cross-validation among cubic b-splines.

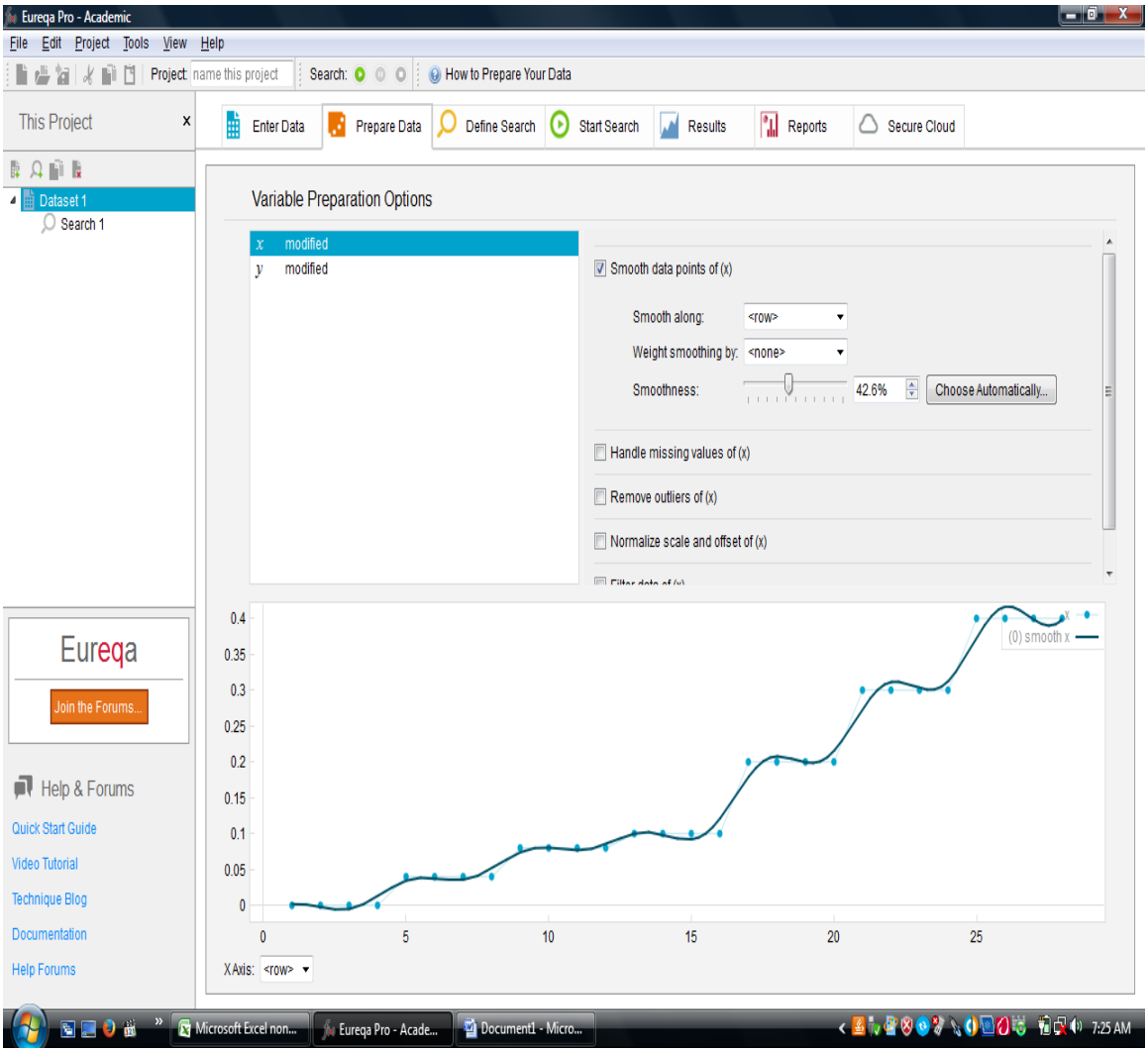


Figure B2: Screen shot of prepare data tab after smoothing x variables

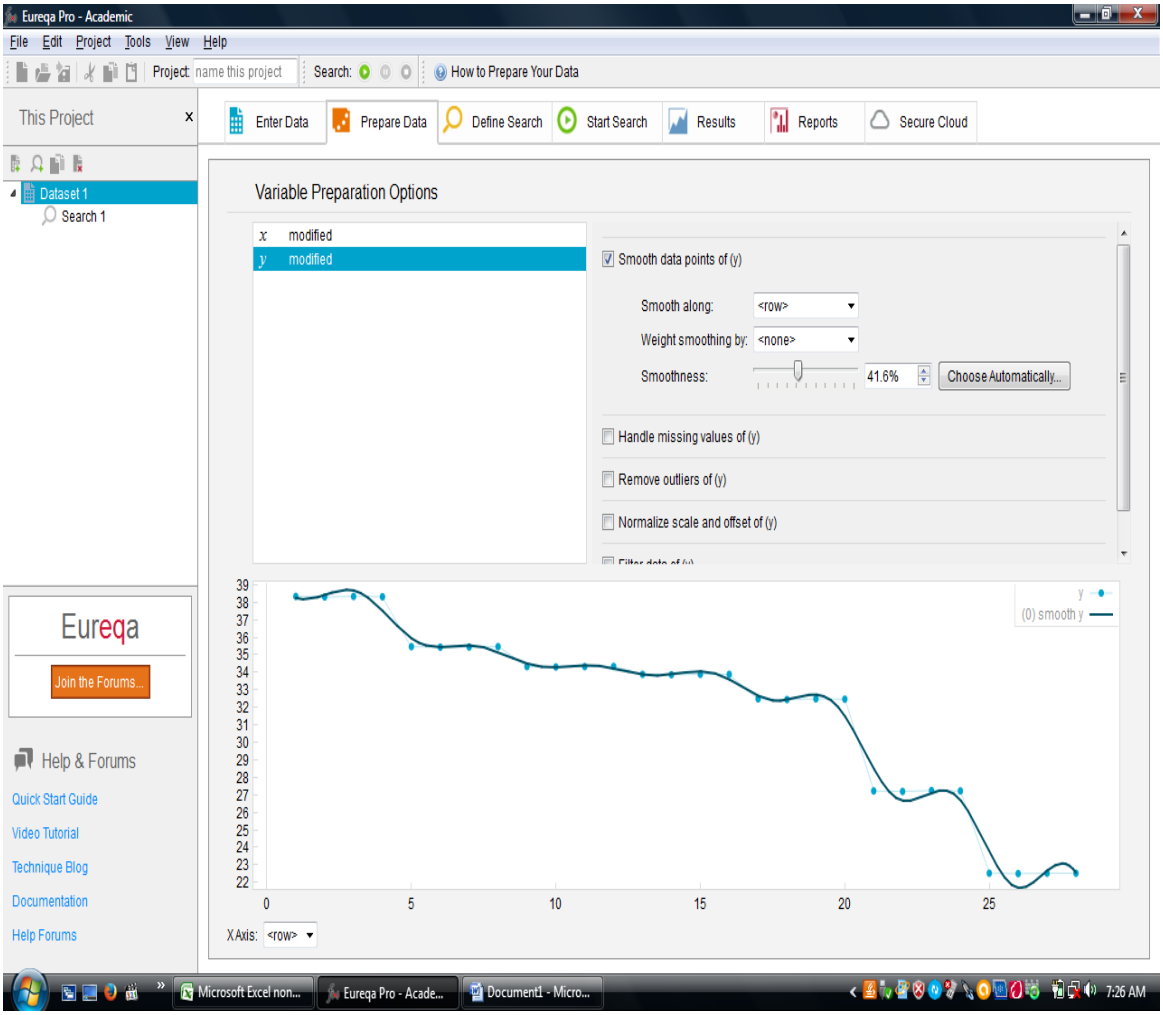


Figure B3: Screen shot of prepare data tab after smoothing y variables

The other options on the prepare data tab were not used because the experimental data has no missing values (the data is continuous without a significant outlier and well scaled).

The pane labelled "define search" suggested a target expression y = f(x), which is exactly what is needed, so no changes were made to it.

The tab also has "Primary Options" with formula building-blocks that can combine in a few trillion ways as it seeks out "good' models. Each building-block has a complexity value that determines how likely it will appear in Eureqa^{TM}'s solution. The lower the complexity value the more likely that it will appear in Eureqa^{TM}'s solution. Similarly, if there are building blocks that one does not want to appear

unless they significantly improve the fit of a solution one may raise the complexity values of those building blocks to make them less likely to appear in the Eureqa™ models.

Since the default checked building-blocks were not sufficient for the sort of expression that is sought, two additional formula building-blocks were checked namely; integer constant and power. The complexity value of power building-block was changed from five to two in order to make it more likely to appear in the model.

The drop-down menu labelled “Error metric” offers different built-in error measures for Eureqa™ to try to optimize. A bound is usually more re-assuring than the other alternatives; worst-case “Maximum error” was chosen. Eureqa™ desktop suggested that “Maximize the R-squared goodness of fit” or “Maximize the correlation coefficient” is more scaled and offset invariant, which are desirable properties too. However, the data is already well scaled.

The “Row weight” drop-down menu is an indicator of how much relative weight one wants Eureqa™ to give to the data in each row. The default row weight showed none, which was retained as each row is important to the formulation of the expected model. For the data splitting drop-down menu, the default was “treat all data point equally” which was also maintained. Figure B4 shows the screen shot of the tab. Not all the formula building-blocks appear in Figure B4.

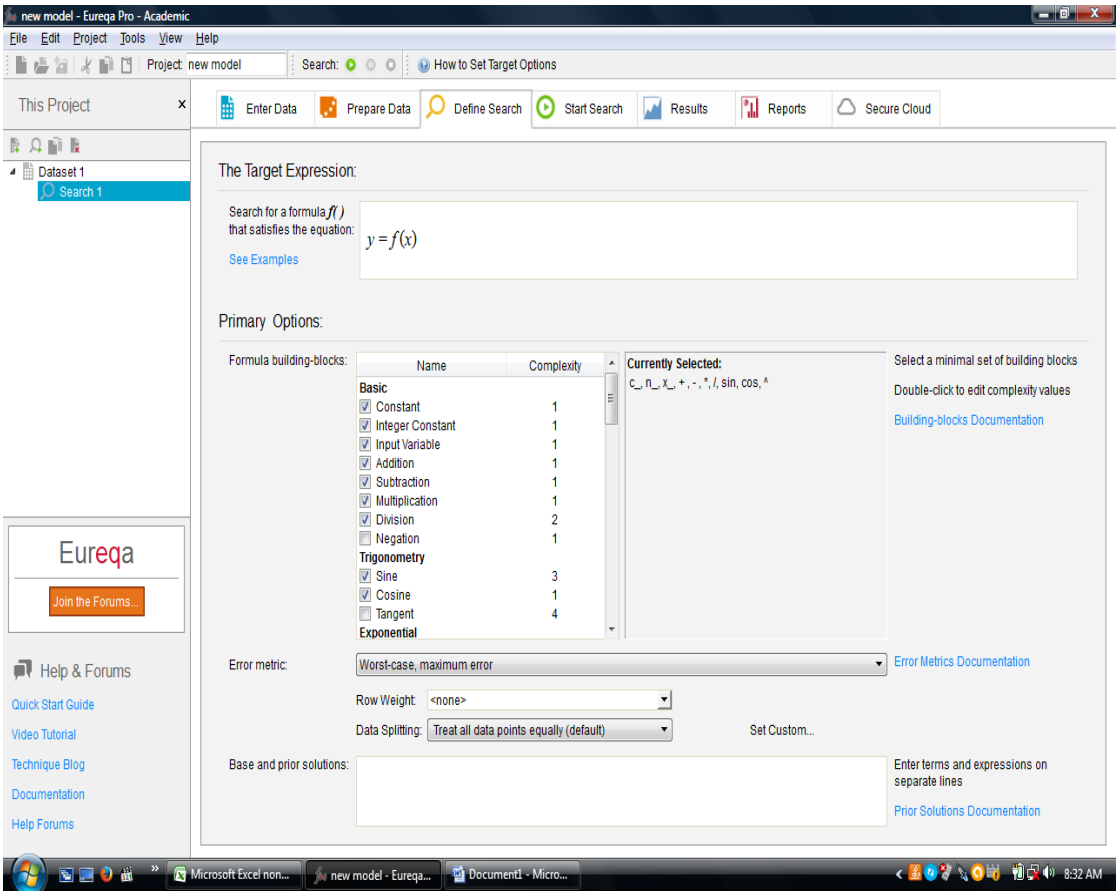


Figure B4: Screen shot of define search tab

The next tab is "Start search" as shown in Figure B5. This tab contains Run, Pause, and Stop buttons. Also, it has Progress and Performance, Progress over time, and Project Log windows. "Progress and Performance" window displays important information about the current search, including the duration of the search, the speed of the search in generations per second and the confidence level in terms of stability and maturity of the solutions.

In the "Progress over time" window, the highest accuracy yet achieved, as determined by the error metric selected in the "Define search" tab, is plotted over the duration of the search. Significant events in the history of the current search, startings, stoppings, and new solution discoveries are recorded in the "Project log" window.

The Run button on the Start Search tab was pressed and the temporal progress of the search was monitored for 10 minutes, 1 second after which the search was stopped.

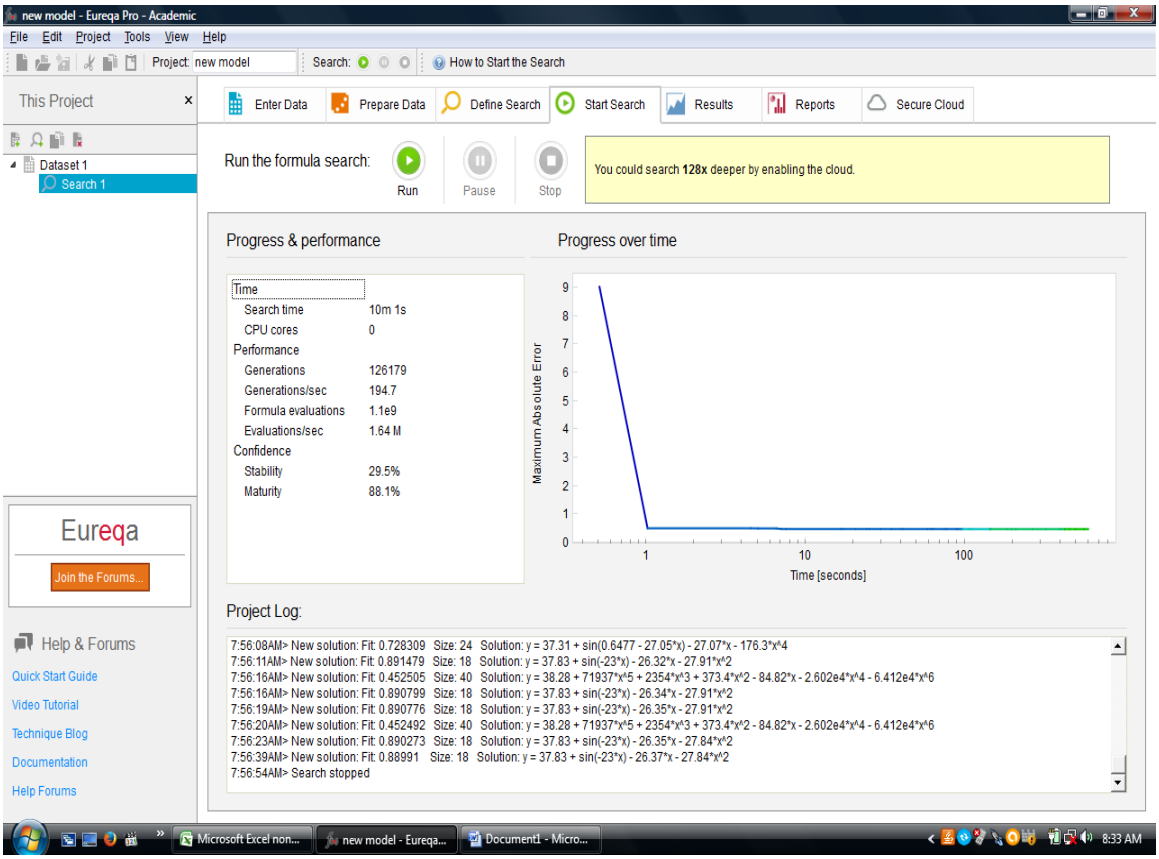


Figure B5: Screen shot of start search tab

Figure B6 shows the results on the "Results tab". This tab contains; best solutions of different sizes, solution fit plot, solution details and solution plotted accuracy vs complexity windows. The best solutions of different sizes window displayed the complexity measure (size), error measure (fit) and their corresponding candidate equation (solution). The solutions were arranged by Eureqa^{TM} based on their complexity to accuracy ratio. "Solution details" window showed the performance metrics of selected equations. The models were subjected to verification and validation. The best model was determined by its complexity and its accuracy.

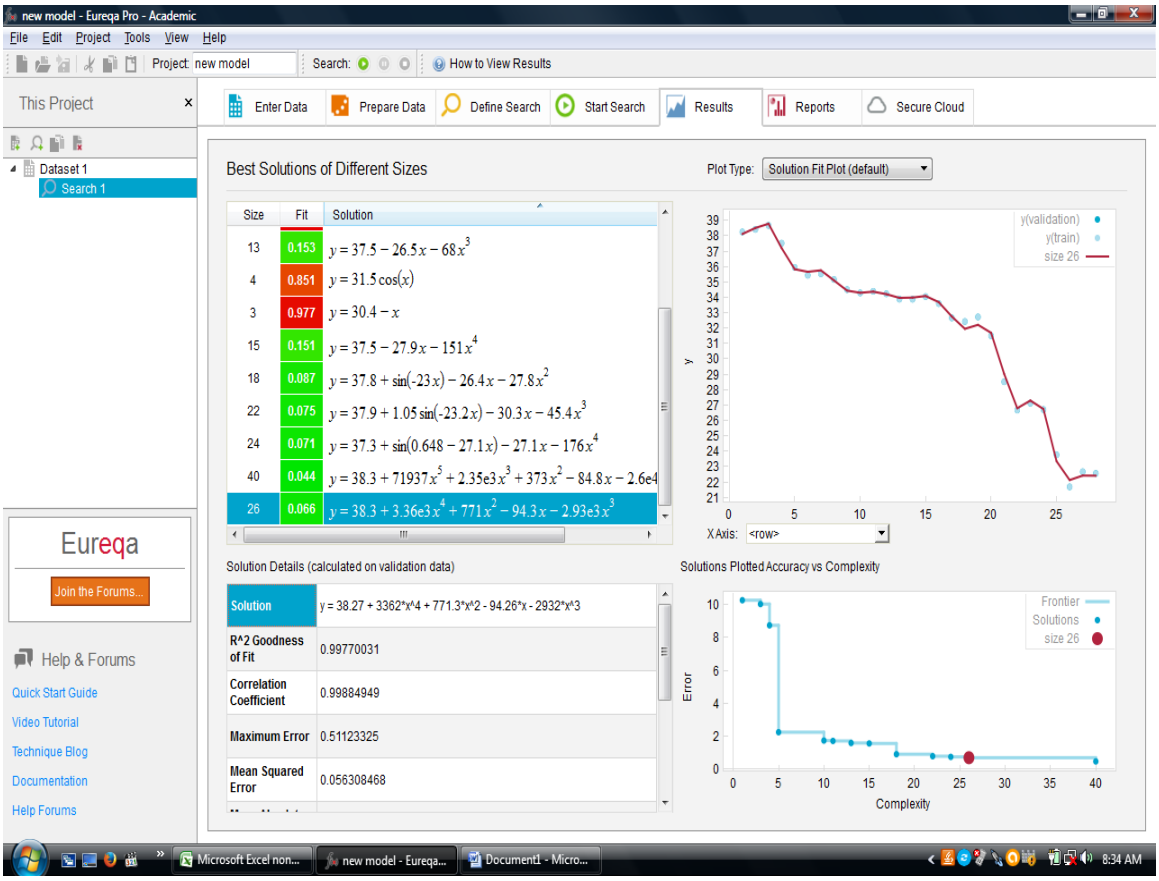


Figure B6: Screen shot of the Result tab

APPENDIX C

MODELS ERROR METRICS

Model 1:

y = 37.79470889 - 36.07853768*x

Data set:

Dataset 1

Error Metrics:

Mean Absolute Error 0.758612

Mean Square Error 0.839368

R2 Goodness of Fit 0.966181

Correlation Coefficient 0.982945

Rank Correlation 0.990148

Maximum Error 1.901

Logarithmic Error 0.478487

Median Error 0.578056

Inter-quartile Absolute Error 0.647605

Signed Difference Error -4.05715e-09

Hybrid Correlation Error 0.206874

Implicit Derivative Error inf

AIC Error 18.676

AUC Error 0

Log Loss Error inf

Hinge Loss Error 0

Model 2:

y = 12.31842694 - 453.631925*cos(4.654864765 + 0.08039215291*x)

Data set:

Dataset 1

Error Metrics:

Mean Absolute Error 0.934221

Mean Square Error 1.14131

R2 Goodness of Fit 0.954015

Correlation Coefficient 0.98296

Rank Correlation 0.990148

Maximum Error 1.5124

Logarithmic Error 0.67375

Median Error 1.01592

Inter-quartile Absolute Error 1.07471

Signed Difference Error -0.548271

Hybrid Correlation Error 0.234861

Implicit Derivative Error inf

AIC Error 73.7008

AUC Error 0

Log Loss Error inf

Hinge Loss Error 0

Model 3:

y = 37.18749693 - 23.87514404*x - 30.71001383*x^2

Data set:

Dataset 1

Error Metrics:

Mean Absolute Error 0.682929

Mean Square Error 0.638644

R2 Goodness of Fit 0.974268

Correlation Coefficient 0.987051

Rank Correlation 0.990148

Maximum Error 1.29593

Logarithmic Error 0.43632

Median Error 0.752826

Inter-quartile Absolute Error 0.700361

Signed Difference Error 0.00590958

Hybrid Correlation Error 0.178153

Implicit Derivative Error inf

AIC Error 57.4446

AUC Error 0

Log Loss Error inf

Hinge Loss Error 0

Model 4:

y = 37.21600795 - 27.13927673*x - 59.78336496*x^3

Data set:

Dataset 1

Error Metrics:

Mean Absolute Error 0.637358

Mean Square Error 0.553781

R2 Goodness of Fit 0.977687

Correlation Coefficient 0.988782

Rank Correlation 0.990148

Maximum Error 1.17011

Logarithmic Error 0.393449

Median Error 0.715073

Inter-quartile Absolute Error 0.651909

Signed Difference Error 0.00738657

Hybrid Correlation Error 0.163543

Implicit Derivative Error inf

AIC Error 53.4524

AUC Error 0

Log Loss Error inf

Hinge Loss Error 0

Model 5:

y = 37.79580174 + 138.714978*x^2 - 48.84996209*x - 283.2283714*x^3

Data set:

Dataset 1

Error Metrics:

Mean Absolute Error 0.525847

Mean Square Error 0.385849

R2 Goodness of Fit 0.984454

Correlation Coefficient 0.992198

Rank Correlation 0.990148

Maximum Error 1.17142

Logarithmic Error 0.285878

Median Error 0.539728

Inter-quartile Absolute Error 0.476139

Signed Difference Error 0.00830126

Hybrid Correlation Error 0.130558

Implicit Derivative Error inf

AIC Error 219.735

AUC Error 0

Log Loss Error inf

Hinge Loss Error 0

Model 6:

y = 38.2823235 + 71941.03593*x^5 + 2354.053738*x^3 + 373.3456236*x^2 - 84.96207994*x - 26021.45232*x^4 - 64121.65887*x^6

Data set:

Dataset 1

Error Metrics:

Mean Absolute Error 0.0741336

Mean Square Error 0.00695913

R2 Goodness of Fit 0.99972

Correlation Coefficient 0.999867

Rank Correlation 0.990148

Maximum Error 0.142342

Logarithmic Error 0.00691513

Median Error 0.0614367

Inter-quartile Absolute Error 0.0683909

Signed Difference Error -0.00403095

Hybrid Correlation Error 0.0153556

Implicit Derivative Error inf

AIC Error 3386.9

AUC Error 0

Log Loss Error inf

Hinge Loss Error 0

Model 7:

y = 38.26698195 + 3361.93668*x^4 + 771.3307281*x^2 - 94.25843653*x - 2932.288779*x^3

Data set:

Dataset 1

Error Metrics:

Mean Absolute Error 0.131866

Mean Square Error 0.0258044

R2 Goodness of Fit 0.99896

Correlation Coefficient 0.999483

Rank Correlation 0.990148

Maximum Error 0.290688

Logarithmic Error 0.0250804

Median Error 0.127819

Inter-quartile Absolute Error 0.114278

Signed Difference Error 0.00638818

Hybrid Correlation Error 0.0281669

Implicit Derivative Error inf

AIC Error 1577.6

AUC Error 0

Log Loss Error inf

Hinge Loss Error 0

APPENDIX D

MODELS SENSITIVITY REPORTS

Variable Sensitivity

$y = 38.28 + 71937*x^5 + 2354*x^3 + 373.4*x^2 - 84.82*x - 2.602e4*x^4 - 6.412e4*x^6$

Variable	Sensitivity	% Positive	Positive Magnitude	% Negative	Negative Magnitude
x	1.1994	0%	0	100%	1.1994

$y = 38.27 + 3362*x^4 + 771.3*x^2 - 94.26*x - 2932*x^3$

Variable	Sensitivity	% Positive	Positive Magnitude	% Negative	Negative Magnitude
x	1.1322	0%	0	100%	1.1322

$y = 37.31 + \sin(0.6477 - 27.05*x) - 27.07*x - 176.3*x^4$

Variable	Sensitivity	% Positive	Positive Magnitude	% Negative	Negative Magnitude
x	1.1216	0%	0	100%	1.1216

$y = 37.87 + 1.053*\sin(-23.16*x) - 30.31*x - 45.36*x^3$

Variable	Sensitivity	% Positive	Positive Magnitude	% Negative	Negative Magnitude
x	1.0332	0%	0	100%	1.0332

$y = 37.83 + \sin(-23*x) - 26.37*x - 27.84*x^2$

Variable	Sensitivity	% Positive	Positive Magnitude	% Negative	Negative Magnitude
x	0.99638	0%	0	100%	0.99638

$y = 37.51 - 27.93*x - 150.7*x^4$

Variable	Sensitivity	% Positive	Positive Magnitude	% Negative	Negative Magnitude
x	0.99845	0%	0	100%	0.99845

$y = 37.49 - 26.46*x - 68*x^3$

Variable	Sensitivity	% Positive	Positive Magnitude	% Negative	Negative Magnitude
x	0.96447	0%	0	100%	0.96447

$y = 37.43 - 22.46*x - 34.01*x^2$

Variable	Sensitivity	% Positive	Positive Magnitude	% Negative	Negative Magnitude
x	0.92703	0%	0	100%	0.92703

y = 56.08*cos(x) - 18.61 - 23.77*x

Variable	Sensitivity	% Positive	Positive Magnitude	% Negative	Negative Magnitude
x	0.93923	0%	0	100%	0.93923

y = 38.38 - 36.29*x

Variable	Sensitivity	% Positive	Positive Magnitude	% Negative	Negative Magnitude
x	1.0053	0%	0	100%	1.0053

y = 31.53*cos(x)

Variable	Sensitivity	% Positive	Positive Magnitude	% Negative	Negative Magnitude
x	0.78282	7%	0.018993	93%	0.84157

y = 30.38 - x

Variable	Sensitivity	% Positive	Positive Magnitude	% Negative	Negative Magnitude
x	1.0053	0%	0	100%	1.0053

EXPLANATION OF TERMS

Sensitivity: The relative impact within this model that a variable has on the target variable.

% Positive: The likelihood that increasing this variable will increase the target variable. If % positive = 70%, then 70% of the time increases in this variable lead to increases in the target variable (but the remaining 30% of the time it either decreases it or has no impact). If % positive = 0%, increases in this variable will not increase the target variable.

Positive Magnitude: When increases in this variable lead to increases in the target variable, this is generally how big the positive impact is.

% Negative: The likelihood that increasing this variable will decrease the target variable. If % negative = 60%, then 60% of the time increases in this variable lead to decreases in the target variable (but the remaining 40% of the time it either increases it or has no impact). If % negative = 0%, increases in this variable will not decrease the target variable.

Negative Magnitude: When increases in this variable lead to decreases in the target variable, this is generally how big the negative impact is.

Details

Given a model equation of the form

$$y = f(x)$$

The influence metrics of x on y are defined as follows:

Sensitivity: $\overline{\left|\frac{\partial y}{\partial x}\right|} . \frac{\sigma(x)}{\sigma(y)}$ evaluated at all input data points.

% Positive: The percent of data points where $\frac{\partial y}{\partial x} > 0$

% Negative: The percent of data points where $\frac{\partial y}{\partial x} < 0$

Positive magnitude: $\overline{\left|\frac{\partial y}{\partial x}\right|} . \frac{\sigma(x)}{\sigma(y)}$ at all points where $\frac{\partial y}{\partial x} > 0$

Negative magnitude: $\overline{\left|\frac{\partial y}{\partial x}\right|} . \frac{\sigma(x)}{\sigma(y)}$ at all points where $\frac{\partial y}{\partial x} < 0$

Where:

$\frac{\partial z}{\partial x}$ = The partial derivate of z with respect to x.

$\sigma(x)$ = The standard deviation of x in the input data.

$\sigma(z)$ = The standard deviation of z

$|x|$ = The absolute value of x

$\bar{x}$ = the mean of x

APPENDIX E

MODELS STATISTICAL REPORTS

Variable Occurrences

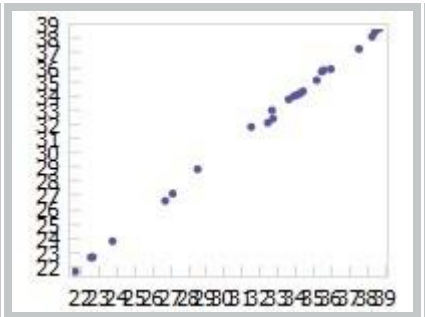
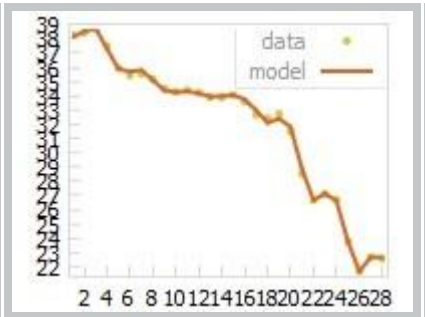
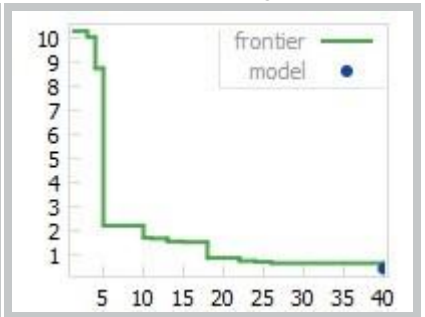
Number of Models each variable appears in

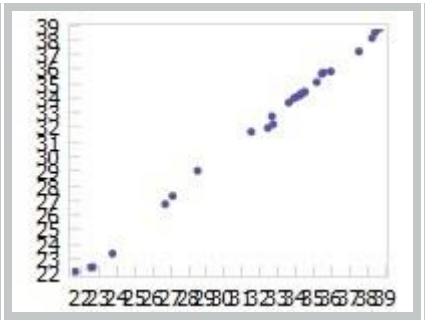
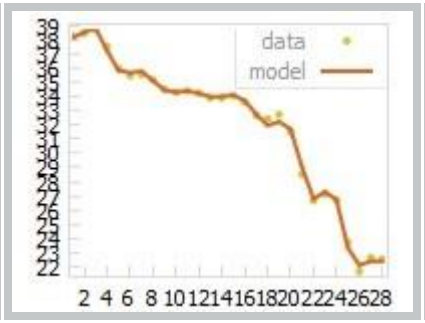
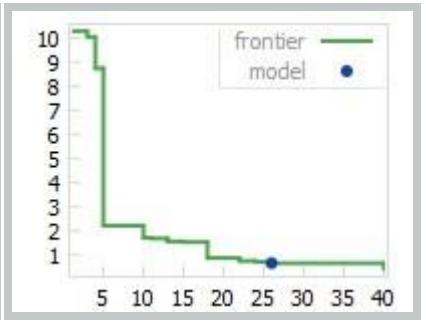
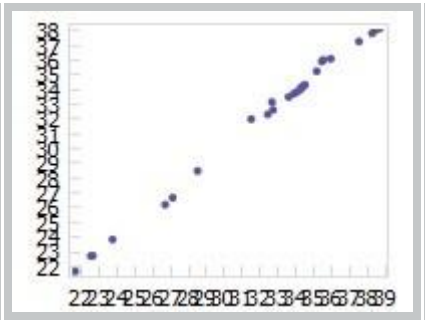
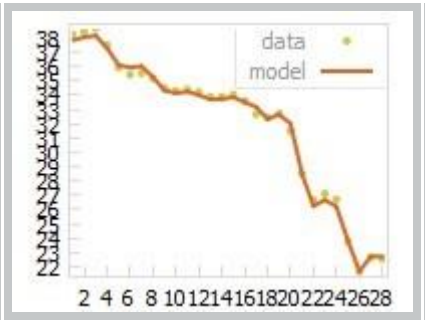
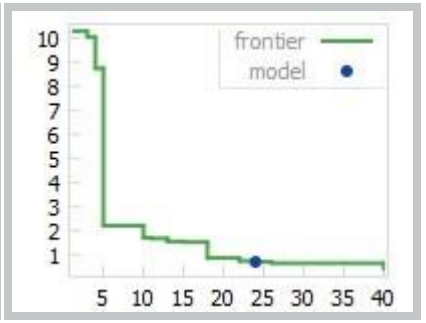
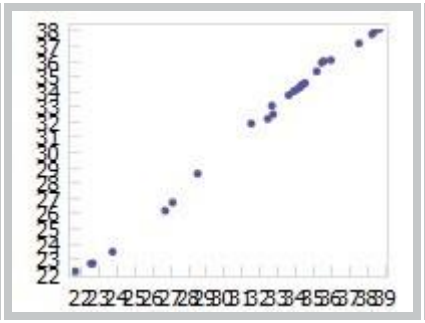
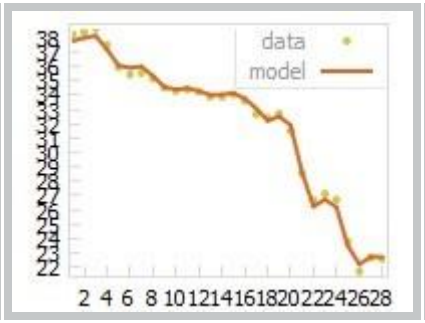
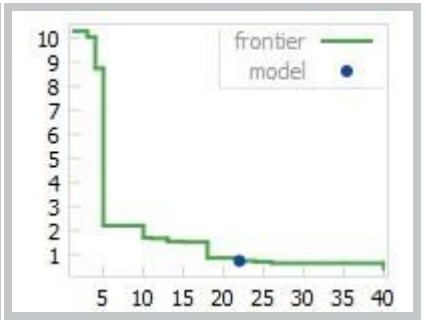


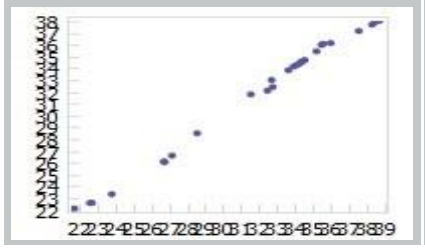
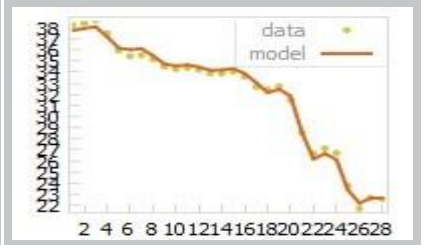
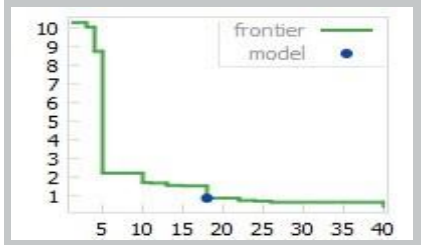
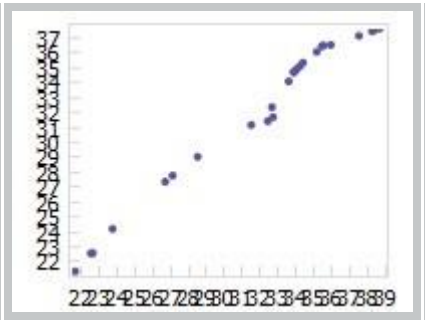
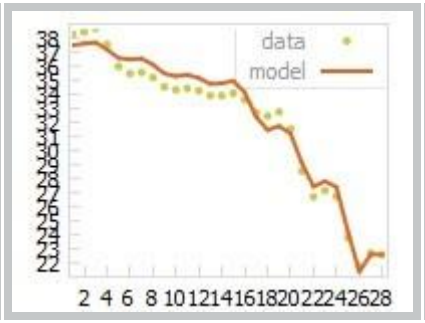
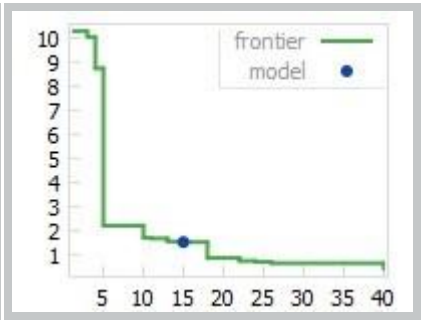
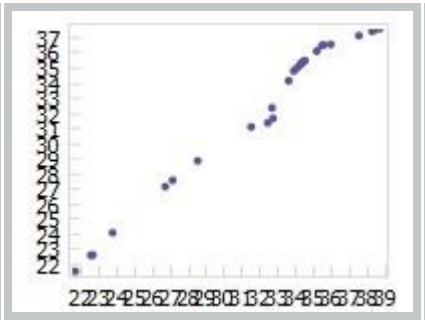
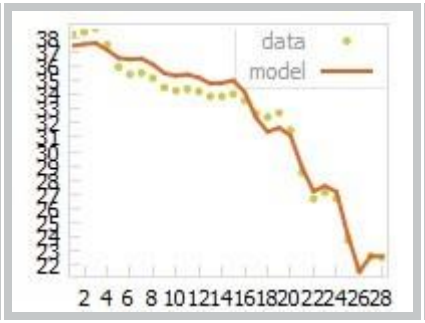
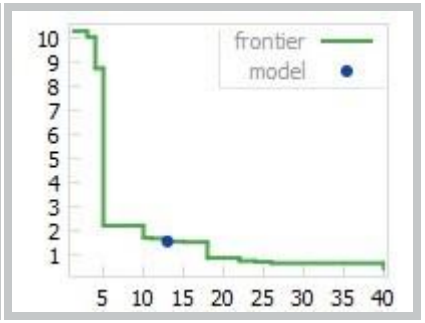
Number of Occurrences of each variable across all models

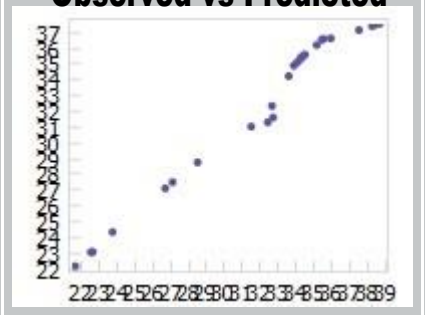
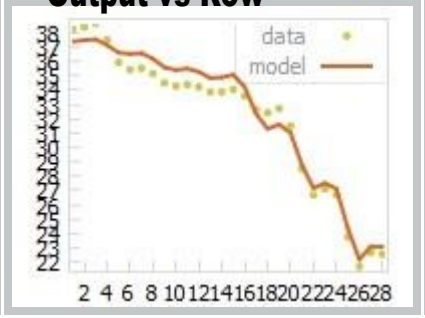
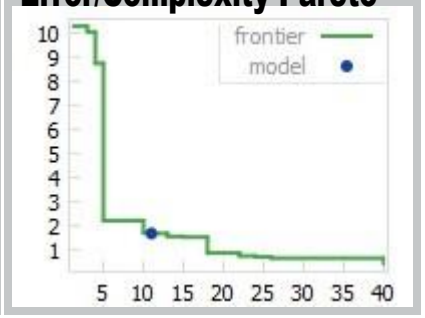
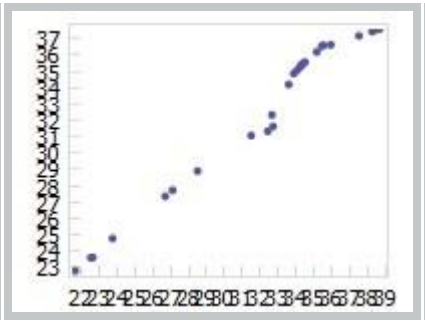
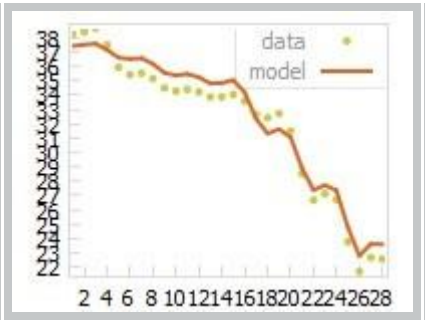
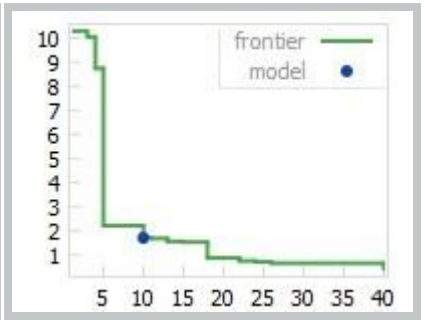
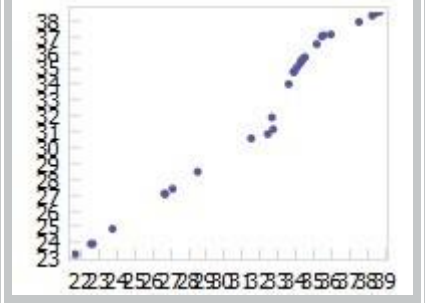
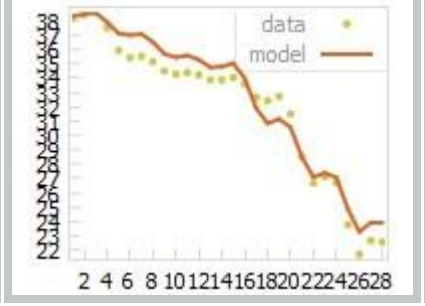
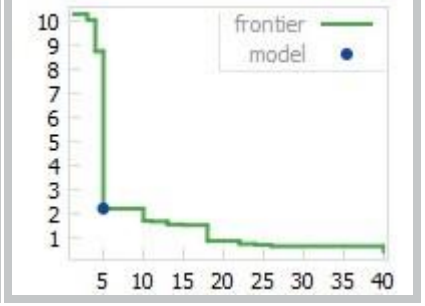


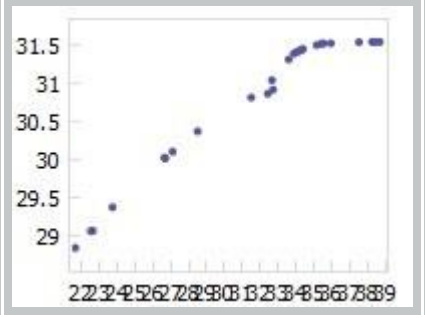
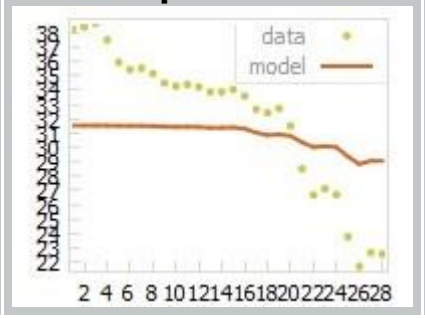
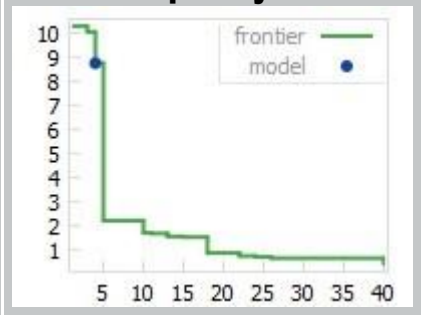
Model List

Model	Observed vs. Predicted	Output vs. Row	Error/Complexity Pareto
Model: $y = a + 71937*x^5 + b*x^3 + c*x^2 - d*x - e*x^4 - f*x^6$ **Text:** `y = 38.2824 + 71937*x^5 + 2354.24*x^3 + 373.369*x^2 - 84.8209*x - 26021.7*x^4 - 64123.4*x^6`			

Model	Observed vs. Predicted	Output vs. Row	Error/Complexity Pareto
Model: $y = a + b*x^4 + c*x^2 - d*x - e*x^3$ **Text:** `y = 38.267 + 3361.94*x^4 + 771.331*x^2 - 94.2584*x - 2932.29*x^3`			
Model: $y = a + \sin(b - c*x) - d*x - e*x^4$ **Text:** `y = 37.3143 + sin(0.647666 - 27.0534*x) - 27.069*x - 176.337*x^4`			
Model: $y = a + b*\sin(-c*x) - d*x - e*x^3$ **Text:** `y = 37.8656 + 1.05294*sin(-23.1551*x) - 30.3129*x - 45.3637*x^3`			

	Observed vs Predicted	Output vs Row	Error/Complexity Pareto
Model: $y = a + \sin(-23*x) - b*x - c*x^2$ **Text:** `y = 37.8275 + sin(-23*x) - 26.3666*x - 27.8408*x^2`			
Model: $y = a - b*x - c*x^4$ **Text:** `y = 37.5072 - 27.9277*x - 150.655*x^4`			
Model: $y = a - b*x - c*x^3$ **Text:** `y = 37.4858 - 26.464*x - 68*x^3`			

	Observed vs Predicted	Output vs Row	Error/Complexity Pareto
Model: $y = a - b*x - c*x^2$ **Text:** `y = 37.4325 - 22.4606*x - 34.0136*x^2`			
Model: $y = a*\cos(x) - b - c*x$ **Text:** `y = 56.0826*cos(x) - 18.6116 - 23.7744*x`			
Model: $y = a - b*x$ **Text:** `y = 38.3758 - 36.2876*x`			

Model: y = a*cos(x) **Text:** `y = 31.531*cos(x)`	**Observed vs Predicted**	**Output vs Row**	**Error/Complexity Pareto**
			
Model: y = a - x **Text:** `y = 30.3804 - x`	